J. Membrane Biol. 118, 19–47 (1990)

The Journal of
Membrane Biology

Inhibition of the Phosphate Self-Exchange Flux in Human Erythrocytes and Erythrocyte Ghosts

F. Stadler and K.F. Schnell
Institut für Physiologie, Universität Regensburg, D-8400 Regensburg, Federal Republic of Germany

Summary. The phosphate self-exchange flux in resealed erythrocyte ghosts and in amphotericin B (5.5 μM) permeabilized erythrocytes has been studied. The phosphate self-exchange flux exhibits an S-shaped concentration dependence and a self-inhibition in permeabilized red cells while in erythrocyte ghosts no self-inhibition of the phosphate flux has been observed. The apparent half-saturation constants and the apparent Hill coefficients were assessed by the double reciprocal Hill plots of $1/\vec{J}_P$ *versus* $1/[P]^n$. The phosphate half-saturation constants amount to approx. 125 mM in ghosts and to about 75 mM in permeabilized cells while the apparent Hill coefficients amount to 1.15 and to 1.65 (pH 7.2, 25°C), respectively. Both chloride and sulfate elicit a mixed-type inhibition of the phosphate self-exchange flux. In permeabilized cells, chloride and sulfate shift the flux optimum towards higher phosphate concentrations and reduce the apparent Hill coefficients. In erythrocyte ghosts, the apparent Hill coefficients are insensitive to these anions. The double reciprocal Hill plots indicate a mixed-type inhibition of the phosphate self-exchange flux by DNDS, salicylate and dipyridamole and a noncompetitive inhibition of the phosphate self-exchange flux by phlorhizin. By contrast, the Hill-Dixon plots for chloride and sulfate indicate a competitive inhibition of the phosphate self-exchange flux in erythrocyte ghosts and a mixed-type inhibition in permeabilized cells and provide Hill coefficients of greater than unity for chloride and sulfate. The Dixon plots for DNDS, salicylate, phlorhizin and dipyridamole show a noncompetitive inhibition of the phosphate flux and provide apparent Hill coefficients of 0.95–1.0 for inhibitor binding. Using the Debye-Hückel theory, the effects of ionic strength upon phosphate transport and inhibitor binding can be eliminated. The results of our studies provide strong evidence for the assumption that electrostatic forces are involved in phosphate transport and in inhibitor binding.

Key Words phosphate · transport · erythrocytes · human

Introduction

Band 3 is the predominant, intrinsic membrane protein of the erythrocyte membrane. Band 3 constitutes a 55-kD membrane domain and a 42-kD cytoplasmic domain which can be split by tryptic digestion. As studied so far, the removal of the cytoplasmic domain has no effect upon anion transport. The membrane domain can be cut by proteolytic enzymes into further fragments, but the dissection or the chemical modification of the membrane domain are associated with changes in anion transport. The membrane domain consists of α-helical loops which span the red cell membrane several times. The hydrophobic segments of the helix appear to be intercalated into the lipid bilayer while the hydrophilic parts are assumed to be located at the membrane surfaces. Thus the band 3 membrane domain could form a channel of appropriate charge and size to catalyze anion transport across the red cell membrane. Band 3 could function as a carrier or as a dielectric pore with fluctuating diffusion barriers. Irrespective of the transport mechanism, anion transport across the erythrocyte membrane is a complex reaction which consists of three consecutive steps. The transported anion first gets bound to the band 3 substrate site. Subsequently, the bound anion is translocated across the red cell membrane and, finally, the transported anion is released at the opposite membrane surface. In terms of the carrier hypothesis, self-inhibition of anion transport at high substrate-anion concentrations has been attributed to the binding of a second substrate-anion to the band 3 modifier site which inhibits the translocation of the bound substrate-anion across the erythrocyte membrane. With regard to the dielectric pore concept, self-inhibition of anion transport results from the blocking of the pore as the *trans*-substrate site of the dielectric pore gets occupied by substrate anions (Schnell, 1977; Tanford, 1985). For reviews *see*: Knauf, 1979; Macara & Cantley, 1983; Jennings, 1985, 1989; Passow, 1986.

Previous studies on the concentration dependence of the phosphate transport in amphothericin B or valinomycin-permeabilized erythrocytes and in resealed erythrocyte ghosts have shown a complex pattern of concentration responsiveness of the phos-

phate transport (Schnell, Besl & von der Mosel, 1981; Schnell & Besl, 1984). The phosphate self-exchange flux in permeabilized red cells and in erythrocyte ghosts exhibited an S-shaped concentration response and provided apparent Hill coefficients of 1.60–1.80 in permeabilized erythrocytes and of about 1.25 in erythrocyte ghosts. Apparent Hill coefficients of greater than unity are indicative to a positive cooperativity of the phosphate self-exchange flux. The cooperativity can result from a cooperative phosphate binding at the membrane surfaces, from a cooperativity of phosphate translocation or from both of these effects. The sigmoidicity of the phosphate flux in erythrocyte ghosts has only been observed at self-exchange conditions, when intracellular and extracellular phosphate concentrations are simultaneously elevated. At homoexchange conditions, intracellular and extracellular phosphate concentrations are separately varied and phosphate concentration at the opposite membrane surface is kept constant. At homoexchange conditions, the sigmoidicity of the concentration dependence of the phosphate flux in erythrocyte ghosts vanishes. These results suggest a cooperativity of phosphate translocation rather than a cooperative phosphate binding at the membrane surfaces. By contrast, chloride self-exchange in erythrocytes and in erythrocyte ghosts is much faster than phosphate self-exchange and displays an entirely different pH dependence (Gunn et al., 1973; Wieth et al., 1973; Dalmark, 1976; Funder & Wieth, 1976; Brahm, 1977; Schnell, Besl & Manz, 1978). Furthermore, the chloride self-exchange fluxes and the chloride homoexchange fluxes in resealed erythrocyte ghosts exhibit simple saturation kinetics and do not provide any evidence for a cooperativity of the chloride transport (Hautmann & Schnell, 1985). Finally, erythrocytes show a self-inhibition of the phosphate and of the chloride self-exchange flux. In erythrocyte ghosts, a self-inhibition of the chloride flux has been found (Funder & Wieth, 1976), but as reported in this paper, no self-inhibition of the phosphate flux in erythrocyte ghosts has been observed. The differences between chloride and phosphate transport are suggestive for differences of the transport mechanism. In contrast to the translocation of chloride, phosphate translocation across the erythrocyte membrane seems to be activated by the binding of a second proton to the phosphate/substrate-site complex which possibly is required for compensation of a negative excess charge that has been introduced by the binding of phosphate to the band 3 substrate site.

This paper is concerned with the concentration dependence and the inhibition of the phosphate self-exchange flux in resealed erythrocyte ghosts and in amphothericin B permeabilized erythrocytes. Phosphate concentrations of 1–250 mM in erythrocyte ghosts and of 10–400 mM in permeabilized erythrocytes have been employed. The Lineweaver-Burk plots for the flux/concentration curves were always curved, but the double recipocal Hill plots and the Hill-Hofstee plots for the phosphate self-exchange in erythrocyte ghosts were linear and provided apparent Hill coefficients of greater than unity. No self-inhibition of the phosphate flux has been detected in erythrocyte ghosts although phosphate concentrations up to 600 mM have been employed. The double-reciprocal Hill plots exhibit a mixed-type inhibition of the phosphate self-exchange flux by chloride and sulfate, by the inhibitors DNDS (4,4′-dinitro-2,2′-stilbene disulfonic acid; K-salt) and salicylate and by the chloride-dependent, cationic inhibitor dipyridamole, but a noncompetitive inhibition of the phosphate self-exchange flux by the inhibitor phlorhizin. By contrast, the Hill-Dixon plots for chloride and for sulfate show a competitive inhibition of the phosphate transport in erythrocyte ghosts and a mixed-type inhibition of the phosphate transport in permeabilized erythrocytes while the Dixon plots for the anion transport inhibitors DNDS, salicylate, dipyridamole and phlorhizin in erythrocyte ghosts all show a noncompetitive type of inhibition of the phosphate self-exchange flux. These controversial results can be brought about by the effects of ionic strength upon phosphate transport and upon inhibitor binding. In order to eliminate ionic strength, special plots have been used which indicate that ionic strength participates in phosphate binding, in inhibitor binding and in phosphate translocation by band 3 protein. The results of our studies provide strong evidence for the assumption that electrostatic forces are involved in phosphate binding to the band 3 substrate site, in phosphate translocation across the erythrocyte membrane and in inhibitor binding to the band 3 protein. These forces can account for the S-shaped concentration dependence, for self-inhibition and for the atypical inhibition of the phosphate self-exchange flux in permeabilized erythrocytes and in resealed erythrocyte ghosts.

Materials and Methods

Preparation of Erythrocytes

Blood from healthy adult donors was used. The blood was withdrawn under sterile conditions and stored for 2–6 days at 4°C. Coagulation was prevented by the addition of ACD solution. Before the experiments, the red blood cells were washed twice in about 20 volumes of 122 mM K-citrate. Plasma and buffy coat were removed. Then 4 g of tightly packed cells (centrifugation 5,000 × g, 10 min, 20°C, pH 7.2) were added to 36 ml of an

isotonic, 132 mM K-phosphate (pH 7.2) and incubated three times for 10 min at 37°C. After depleting the cells of chloride, the cells were transferred into a K-phosphate/sucrose solution (pH 7.2, 37°C) containing 110 mM phosphate, 30 mM sucrose and 5.5 μM amphotericin B. Phosphate then was slowly titrated to the required concentrations by adding 30 mM sucrose or 1043 mM K-phosphate. Care must be exercised to avoid hemolysis of the red cells. Extracellular phosphate was monitored by photometric determination of inorganic phosphate. 30 mM sucrose had been added in order to counterbalance the osmotic pressure of hemoglobin. After titration, the cells were spun down, the supernatant was removed and the permeabilized red cells were resuspended in 10–400 mM K-phosphate, 30 mM sucrose (pH 7.2, 37°C) and labeled with ^{32}P-phosphate. Each sample then was subdivided into two portions. Portion 1 had been used for the flux measurements. Portion 2 was destined for measuring the phosphate equilibrium distribution and was labeled additionally with 10 mM D(1-^{3}H)-glucose. No attempts were made to remove amphotericin B quantitatively from the red blood cells.

Preparation of Erythrocyte Ghosts

Erythrocyte ghosts were prepared from ACD blood which had been stored for 2–6 days at 4°C. In order to completely remove intracellular chloride, the red blood cells were preincubated three times for 10 min in 20 volumes of 132 mM K-phosphate (37°C, pH 7.2, 330 mosM) and the buffy coat was removed. Then 1 g of tightly packed erythrocytes was resuspended within 1 ml 122 mM K-citrate to make up a 50% (wt/vol) erythrocyte suspension. The erythrocytes were osmotically hemolyzed at 0°C, pH 6.2, by adding 20 ml of a hypotonic 15 mosM citrate solution (2 mM trimagnesium dicitrate, 3.8 mM citric acid) to 2 ml of the erythrocyte suspension. Five min after hemolysis, 6.5 ml of a hypertonic K-phosphate/K-citrate/sucrose solution (2640 mosM) were added to the hemolysate and the erythrocyte ghosts then were resealed by incubating them for 45 min at 37°C, pH 7.2 in a double isotonic solution (660 mosM). The resealing solution contained 1–250 mM K-phosphate, 40 mM K-citrate and different concentrations of sucrose for isosmotic substitution up to 660 mosM. The phosphate solutions were supplemented with tracer amounts of ^{32}P-phosphate. In order to cover a greater range of phosphate concentrations all experiments were performed in double isotonic solutions except for the phosphate flux measurements in the presence of chloride and sulfate where a higher tonicity had been used. The osmolarity of the solutions was checked by means of a microosmometer. The following solutions have a tonicity of 660 mosM: 530 mM sucrose, 325 mM K-phosphate and 323 mM K-citrate. The yield of resealed erythrocyte ghosts amounts to approx. 90% of the hemolyzed red cells.

Determination of V_i, $[P]_i$ and $[Cl]_i$

The intracellular volume, V_i, the intracellular phosphate concentration $[P]_i$ and the intracellular chloride concentration $[Cl]_i$ were assessed by using a double-label technique which permits a simultaneous counting of ^{32}P-phosphate or of ^{36}Cl-chloride and D(1-^{3}H)-glucose, respectively. The phosphate solutions were supplemented with 10 mM D(1-^{3}H)-glucose and 1 mM ^{36}Cl-chloride. D(1-^{3}H)-glucose was used as a marker of intracellular volume. The equilibrium distribution of D(1-^{3}H)-glucose between intracellular and extracellular space is close to unity and has been checked by counting intracellular D(1-^{3}H)-glucose and gravimetric determination of intracellular water. In erythrocytes, the ratio of $[^3\text{H-CPM}]_i/[^3\text{H-CPM}]_e$ was 1.04 ± 0.05 (mean ± SD, 25 experiments) while in erythrocyte ghosts, $[^3\text{H-CPM}]_i/[^3\text{H-CPM}]_e$ was 1.03 ± 0.05 (mean ± SD, 20 experiments). The equilibrium distribution of D(1-^{3}H)-glucose in erythrocytes and in erythrocyte ghosts remains constant for at least 60 min. ^{36}Cl-chloride has been employed as a reference anion. The intracellular volume, V_i, the intracellular phosphate concentration, $[P]_i$, and the intracellular chloride concentration, $[Cl]_i$, were calculated as follows:

$$V_i = (^3\text{H-CPM}_i/^3\text{H-CPM}_e)V_e \quad (1)$$

$$[P]_i = ((^{32}\text{P-CPM}_i/^3\text{H-CPM}_i)/(^{32}\text{P-CPM}_e/^3\text{H-CPM}_e))[P]_e \quad (2)$$

$$[Cl]_i = ((^{36}\text{Cl-CPM}_i/^3\text{H-CPM}_i)/(^{36}\text{Cl-CPM}_e/^3\text{H-CPM}_e))[Cl]_e. \quad (3)$$

^{32}P-CPM, ^{36}Cl-CPM, and ^{3}H-CPM are the radioactivity of ^{32}P-phosphate, ^{36}Cl-chloride and D(1-^{3}H)-glucose. [P] and [Cl] are the phosphate and the chloride concentrations. The subscripts i and e refer to intracellular and to the extracellular space. V_i and V_e are the intracellular and the extracellular volume.

Flux Measurements

All flux measurements were executed at self-exchange conditions when extracellular and intracellular phosphate except for the tracer are at equilibrium. The flux experiments were performed with 10% (wt/vol) suspensions of ^{32}P-phosphate-labeled erythrocytes or erythrocyte ghosts. Intracellular phosphate, n_{iP} (mol/g cells) was calculated by using Eq. (4). ^{32}P-CPM is the intracellular ^{32}P-phosphate and $[^{32}\text{P-CPM}]_e/[P]_e$ is the specific activity of extracellular phosphate:

$$n_{iP} = {}^{32}\text{P-CPM}_i/([^{32}\text{P-CPM}_e]/[P]_e). \quad (4)$$

For that purpose, aliquots were taken from the suspensions of ^{32}P-phosphate-labeled erythrocytes and erythrocyte ghosts. The erythrocyte ghosts and the erythrocytes were washed twice with approximately 100 volumes of nonradioactive, 660 mosM phosphate/citrate/sucrose solution (4°C, pH 7.2) supplemented by 1 mM DNDS. Subsequently, the erythrocyte ghosts and the red blood cells were lysed by small quantities of saponin, protein was removed by trichloracetic acid and intracellular ^{32}P-phosphate then was counted. The concentration of extracellular phosphate was checked by photometric determination of inorganic phosphate (Merckotest 3331).

Before starting the ^{32}P-phosphate efflux measurements, the trapped, extracellular ^{32}P-phosphate was removed by washing the ^{32}P-phosphate-labeled erythrocytes and erythrocyte ghosts once with about 50 volumes of a nonradioactive, 660 mosM K-phosphate/K-citrate/sucrose solution (4°C, pH 7.2). The ^{32}P-phosphate back exchange then was initiated by resuspending the ^{32}P-phosphate-labeled erythrocytes or erythrocyte ghosts in nonradioactive K-phosphate/K-citrate/sucrose solution (pH 7.2, 25°C) and measuring the extracellular ^{32}P-phosphate at appropriate time intervals. At self-exchange conditions, the ^{32}P-phosphate back exchange is a first-order reaction and the rate constant, k (min)$^{-1}$, of the ^{32}P-phosphate efflux is obtained by fitting the curves of extracellular ^{32}P-CPM *versus* time to:

$$\ln(^{32}\text{P-CPM}_\infty - {}^{32}\text{P-CPM}) = -kt + \ln(^{32}\text{P-CPM}_\infty - {}^{32}\text{P-CPM}_o). \quad (5)$$

^{32}P-CPM, ^{32}P-CPM$_o$ and ^{32}P-CPM$_\infty$ are the extracellular ^{32}P-phos-

Table 1. Double-reciprocal Hill plot of $1/\vec{J}_P$ *versus* $1/[P]^n$ *

Competitive inhibition	
$K^n_{P(app)} = K^n_P(1 + [I]^m/K_i^m)$	$\vec{J}_{max(app/P)} = \vec{J}_{max(P)}$
IP: $1/[P]^n = 0$	$1/\vec{J}_P = 1/\vec{J}_{max(P)}$
Competitive inhibition with linear self-inhibition	
$K^n_{P(app)} = \dfrac{K^n_{iP}K^n_P(1 + [I]^m/K_i^m)}{K^n_{iP} + K^n_P(1 + [I]^m/K_i^m)}$	$\vec{J}_{max(app/P)} = \dfrac{\vec{J}_{max(P)}K^n_{iP}}{K^n_{iP} + K^n_P(1 + [I]^m/K_i^m)}$
IP: $1/[P]^n = -1/K^n_{iP}$	$1/\vec{J}_P = 1/\vec{J}_{max(P)}$
Noncompetitive inhibition	
$K^n_{P(app)} = K^n_P$	$\vec{J}_{max(app/P)} = \vec{J}_{max(P)}/(1 + [I]^m/K_i^m)$
IP: $1/[P]^n = -1/K^n_P$	$1/\vec{J}_P = 0$
Noncompetitive inhibition with linear self-inhibition	
$K^n_{P(app)} = \dfrac{K^n_PK^n_{iP}}{K^n_P + K^n_{iP}}$	$\vec{J}_{max(app/P)} = \dfrac{\vec{J}_{max(P)}K^n_{iP}}{(K^n_P + K^n_{iP})(1 + [I]^m/K_i^m)}$
IP: $1/[P]^n = -K^n_PK^n_{iP}/(K^n_P + K^n_{iP})$	$1/\vec{J}_P = 0$
Mixed-type inhibition	
$K^n_{P(app)} = K^n_P\dfrac{1 + [I]^m/K_i^m}{1 + [I]^m/K_{ii}^m}$	$\vec{J}_{max(app/P)} = \dfrac{\vec{J}_{max(P)}}{1 + [I]^m/K_{ii}^m}$
IP: $1/[P]^n = -K_i^m/(K^n_PK_{ii}^m)$	$1/\vec{J}_P = (1 - K_i^m/K_{ii}^m)/\vec{J}_{max(P)}$
Mixed-type inhibition with linear self-inhibition	
$K^n_{P(app)} = \dfrac{K^n_PK^n_{iP}(1 + [I]^m/K_i^m)}{K^n_P(1 + [I]^m/K_i^m) + K^n_{iP}(1 + [I]^m/K_{ii}^m)}$	$\vec{J}_{max(app/P)} = \dfrac{\vec{J}_{max(P)}K^n_{iP}}{K^n_P(1 + [I]^m/K_i^m) + K^n_{iP}(1 + [I]^m/K_{ii}^m)}$
IP: $1/[P]^n = -\dfrac{K^n_PK_{ii}^m + K^n_{iP}K_i^m}{K^n_PK^n_{iP}K_{ii}^m}$	$1/\vec{J}_P = (1 - K_i^m/K_{ii}^m)/\vec{J}_{max(P)}$

* The apparent phosphate half-saturation constant, $K_{P(app)}$, the apparent maximal phosphate self-exchange flux, $\vec{J}_{max(app/P)}$, from the $1/[P]^n$- and the $1/\vec{J}_P$-axis intercepts and the intersection points (IP) of the double reciprocal Hill plots are given in the Table. For the calculation of the intersection points the $[P]^{2n}$-terms in the denominator of the Hill equations have been neglected. $\vec{J}_P$ and $\vec{J}_{max(P)}$ are the unidirectional and the maximal unidirectional phosphate flux, K_P and K_{iP} are the half-saturation and the self-inhibition constants of phosphate and K_i is the inhibition constant. [P] and [*I*] are the phosphate and the inhibitor concentrations, *n* and *m* are the apparent Hill coefficients for phosphate and for the inhibitor, respectively.

phate at time *t*, at zero time and at infinite time. The unidirectional phosphate self-exchange flux, $\vec{J}_P$ (mol/(min · g cells)), then is given by:

$$\vec{J}_P = k \cdot n_{iP}. \tag{6}$$

The phosphate self-exchange fluxes all are expressed in mol/(min · g cells) where 1 g cells refers to the wet weight of erythrocytes at standard conditions (centrifugation: 10 min, 5,000 × *g*, pH 7.2, 20°C) and corresponds to 1.10×10^{10} erythrocytes.

Plotting Procedures

The phosphate self-exchange flux in permeabilized red blood cells and in resealed erythrocyte ghosts provided S-shaped flux/concentration curves with a self-inhibition of the phosphate flux at high phosphate concentrations. The S-shaped flux/concentration and the S-shaped dose-response curves can be fitted to modified Hill equations if appropriate extensions are made. The extensions are based upon the following assumptions: (*i*) For translocation across the erythrocyte membrane phosphate gets bound to the band 3 substrate site. (*ii*) Competitive inhibitors interact with the band 3 substrate site and inhibit the binding of phosphate to the substrate site. (*iii*) Noncompetitive inhibitors bind to a band 3 inhibitor site and prevent the translocation of bound phosphate. (*iv*) A mixed-type inhibitor requires two binding sites and acts partially as a competitive and partially as a noncompetitive inhibitor. (*v*) The self-inhibition of the phosphate flux at high phosphate concentrations is caused by the binding of a second phosphate anion to the band 3 modifier site which in turn elicits a noncompetitive inhibition of the phosphate flux. The Hill equations for a competitive, a noncompetitive and a mixed-type inhibition read as shown by Eqs. (7)–(9):

Table 2. Hill-Dixon plot of $1/\vec{J}_P$ *versus* $[I]^m$ *

Competitive inhibition	
$K^m_{i(app)} = K^m_i(1 + [P]^n/K^n_P)$	$\vec{J}_{P(o)} = \vec{J}_{max(P)}[P]^n/(K^n_P + [P]^n)$
IP: $[I]^m = -K^m_i$	$1/\vec{J}_P = 1/\vec{J}_{max(P)}$
Competitive inhibition with linear self-inhibition	
$K^m_{i(app)} = K^m_i \dfrac{K^n_P(1 + [P]^n/K^n_{iP}) + [P]^n}{K^n_P(1 + [P]^n/K^n_{iP})}$	$\vec{J}_{P(o)} = \dfrac{\vec{J}_{max(P)}[P]^n}{K^n_P(1 + [P]^n/K^n_{iP}) + [P]^n}$
IP: $[I]^m = -K^m_i$	$1/\vec{J}_P = 1/\vec{J}_{max(P)}$
Noncompetitive inhibition	
$K^m_{i(app)} = K^m_i$	$\vec{J}_{P(o)} = \vec{J}_{max(P)}[P]^n/(K^n_P + [P]^n)$
IP: $[I]^m = -K^m_i$	$1/\vec{J}_P = 0$
Noncompetitive inhibition with linear self-inhibition	
$K^m_{i(app)} = K^m_i$	$\vec{J}_{P(o)} = \vec{J}_{max(P)}[P]^n/(K^n_P(1 + [P]^n/K^n_{iP}) + [P]^n)$
IP: $[I]^m = -K^m_i$	$1/\vec{J}_P = 0$
Mixed-type inhibition	
$K^m_{i(app)} = K^m_i K^m_{ii} \dfrac{K^n_P + [P]^n}{K^m_i[P]^n + K^m_{ii}K^n_P}$	$\vec{J}_{P(o)} = \dfrac{\vec{J}_{max(P)}[P]^n}{K^n_P + [P]^n}$
IP: $[I]^m = -K^m_i$	$1/\vec{J}_P = (1 - K^m_i/K^m_{ii})/\vec{J}_{max(P)}$
Mixed-type inhibition with linear self-inhibition	
$K^m_{i(app)} = \dfrac{K^m_i K^m_{ii}(K^n_P(1 + [P]^n/K^n_{iP}) + [P]^n)}{K^m_i[P]^n + K^m_{ii}K^n_P(1 + [P]^n/K^n_{iP})}$	$\vec{J}_{P(o)} = \dfrac{\vec{J}_{max(P)}[P]^n}{K^n_P(1 + [P]^n/K^n_{iP}) + [P]^n}$
IP: $[I]^m = -K^m_i$	$1/\vec{J}_P = (1 - K^m_i/K^m_{ii})/\vec{J}_{max(P)}$

* $K_{i(app)}$, the apparent inhibition constant, $\vec{J}_{P(o)}$, the control flux at zero inhibitor from the $[I]$-axis and the $1/\vec{J}_P$-axis intercepts, and the coordinates of the intersection points (IP) are given in the Table. The $[P]^{2n}$-term in the denominator of the Hill equations has been neglected.

Table 3. Plot of $\log(i/(i_{max}-i))$ *versus* $\log[I]$*

Competitive inhibition	
$\log(i/(i_{max}-i)) = m \log[I] - \log(K^m_i(1 + [P]^n/K^n_P))$	
For $\log(i/(i_{max}-i)) = 0$:	$m \log[I]_{0.5} = \log(K^m_i(1 + [P]^n/K^n_P))$
Noncompetitive inhibition	
$\log(i/(i_{max}-i)) = m \log[I] - \log(K^m_i)$	
For $\log(i/(i_{max}-i)) = 0$:	$m \log[I]_{0.5} = \log(K^m_i)$
Mixed-type inhibition	
$\log(i/(i_{max}-i)) = m \log[I] - \log((K^m_i K^m_{ii}(K^n_P + [P]^n)/(K^m_{ii}K^n_P + K^m_i[P]^n))$	
For $\log(i/(i_{max}-i)) = 0$:	
$m \log[I]_{0.5} = \log((K^m_i K^m_{ii}(K^n_P + [P]^n)/(K^m_{ii}K^n_P + K^m_i[P]^n))$	

* $i = (1 - \vec{J}_{P(i)}/\vec{J}_{P(o)})$ and $i_{max} = (1 - \vec{J}_{P(ir)}/\vec{J}_{P(o)})$ are the fractional and the maximal fractional inhibition of the flux. $\vec{J}_{P(o)}$ is the phosphate flux at zero inhibitor, $\vec{J}_{P(i)}$ is the flux in the presence of an inhibitor, $\vec{J}_{P(ir)}$ is the inhibitor-insensitive residual phosphate flux and $[I]$ is the inhibitor concentration. The plots of $\log(i/(i_{max}-i))$ *versus* $\log[I]$ gives m, the apparent Hill coefficient for the inhibitor, $\log[I]_{0.5}$ and i_{max}, the maximal fractional inhibition of the flux. With regard to the plots of $\log(i/(i_{max}-i))$ *versus* $\log[I]$, self-inhibition cancels out.

$$\vec{J}_P = \frac{\vec{J}_{max(P)}[P]^n}{(K_P^n(1 + [I]^m/K_i^m) + [P]^n)(1 + [P]^n/K_{iP}^n)} \quad (7)$$

$$\vec{J}_P = \frac{\vec{J}_{max(P)}[P]^n}{(K_P^n + [P]^n)(1 + [I]^m/K_i^m)(1 + [P]^n/K_{iP}^n)} \quad (8)$$

$$\vec{J}_P = \frac{\vec{J}_{max(P)}[P]^n}{(K_P^n(1 + [I]^m/K_i^m) + [P]^n)(1 + [I]^m/K_{ii}^m))(1 + [P]^n/K_{iP}^n)} \quad (9)$$

[P], [I] —phosphate and inhibitor concentration
K_P, K_{iP} —half-saturation and self-inhibition constants
K_i, K_{ii} —inhibition constants
$\vec{J}_P$, $\vec{J}_{max(P)}$—unidirectional phosphate self-exchange flux and maximal unidirectional phosphate self-exchange flux
n, m —Hill coefficient for phosphate self-exchange flux and for inhibitor binding.

The flux/concentration curves of the phosphate self-exchange flux have been fitted to the plot of $1/\vec{J}_P$ *versus* $1/[P]^n$ and to the plot of $\vec{J}_P$ *versus* $\vec{J}_P/[P]^n$ which correspond to the Lineweaver-Burk and to the Woolf-Augustinsson-Hofstee plot and are referred to here as the double-reciprocal Hill plot and the Hill-Hofstee plot. Both plots give similar results but the Hill-Hofstee plot is not suited for the presentation of the data. The flux/concentration curves were analyzed by fitting the ascending branches of the flux/concentration curves to the double-reciprocal Hill plot or to the Hill-Hofstee plot. The term $(1 + [P]^n/K_{iP}^n)$ in the denominator of Eqs. (7)–(9) refers to the self-inhibition of the unidirectional phosphate flux at high phosphate concentrations. At $[P]^n \ll (K_P^n + K_{iP}^n)$, the $[P]^{2n}$-term in the denominator of Eqs. (7)–(9) can be disregarded and self inhibition becomes linear. For curve fitting, n was varied until the double reciprocal Hill plots or the Hill-Hofstee plots became linear. In general, correlation coefficients, r^2, of greater than 0.998 have been attained. The apparent phosphate half-saturation constant, $K_{P(app)}^n$, the apparent maximal unidirectional phosphate flux, $\vec{J}_{max(app/P)}$, and the coordinates of the intersection points of the double reciprocal Hill plots are summarized in Table 1. A linear self-inhibition cannot be perceived by systematic deviations in the double reciprocal Hill plot or the Hill-Hofstee plot and can result in an underestimate of $K_{P(app)}$ and $\vec{J}_{max(app/P)}$ and in an overestimate of the apparent Hill coefficient n.

Since in most cases only a few points are available on the descending branches of the flux/concentration curves, the estimate of the apparent phosphate self-inhibition constants is difficult. If the phosphate half-saturation constant is known, an estimate of the self-inhibition constant can best be made from the position of the flux-optimum of the phosphate self-exchange flux. The relation between the phosphate concentration, $[P]_{opt}$, at the flux optimum, the apparent half-saturation constant, $K_{P(app)}$ and the self-inhibition constant, $K_{iP(app)}$ is given by (Schnell et al., 1981):

$$[P_{opt}]^2 = K_{P(app)} \cdot K_{iP(app)}. \quad (10)$$

The dose-response curves of the phosphate self-exchange flux have been fitted to the Dixon plots of $1/\vec{J}_P$ *versus* $[I]$, to the Hill-Dixon plots of $1/\vec{J}_P$ *versus* $[I]^m$, or to the double logarithmic plot of $\log(i/(i_{max}\text{-}i))$ *versus* $\log[I]$. $i = 1 - \vec{J}_{P(i)}/\vec{J}_{P(o)}$, is the fractional inhibition, $i_{max} = 1 - \vec{J}_{P(ir)}/\vec{J}_{P(o)}$, is the maximal fractional inhibition of the phosphate self-exchange flux. $\vec{J}_{P(i)}$ and $\vec{J}_{P(o)}$ are the phosphate self-exchange flux in the presence of inhibitor and at zero inhibitor, $\vec{J}_{P(ir)}$ is the inhibitor-insensitive residual phosphate flux and $[I]$ is the inhibitor concentration. For a true competitive inhibition or for a mixed-type inhibition the Hill-Dixon plots intersect above the $[I]^m$-axis while for a true noncompetitive inhibition, the Hill-Dixon plots intersect on the $[I]^m$-axis. Hyperbolic Dixon plots indicate an inhibitor-insensitive residual flux and become linear upon subtraction of a suitable residual flux. Parabolic Dixon plots are indicative of a cooperative inhibitor binding and can be fitted to the Hill-Dixon plots. $K_{i(app)}$, the apparent inhibition constant from the $[I]^m$-axis, $\vec{J}_{P(o)}$ from the $1/\vec{J}_P$-axis intercept and the coordinates of the intersection points for the different Hill-Dixon plots are listed in Table 2. For the fit of the dose-response curves to the double logarithmic plot of $\log(i/(i_{max}\text{-}i))$ *versus* $\log[P]$, i_{max} was varied until the plot was linear. The slope of the double logarithmic plot is independent of the residual flux and gives the apparent Hill coefficient for the inhibitor (Table 3).

Chemicals

K_2HPO_4, KH_2PO_4, KCl, NaCl, K-citrate and citric acid of pa grade, sucrose, saponin and Merckotest 3331 for photometric determination of inorganic phosphate were bought from Merck. ^{32}P-phosphate and D(1-^{3}H)-glucose were supplied by Amersham-Buchler, DIDS (4,4′-diisothiocyanato-2,2′-disulfonatostilbene, K-salt) was synthesized in our laboratory (purity >98%). DNDS (4,4′-dinitro-2,2′-stilbenedisulfonic acid, K-salt), salicylate, phlorhizin and dipyridamole were purchased from ICN Pharmaceuticals, Merck, Roth KG and Sigma. The pK of phlorhizin and of dipyridamole were assessed by titration. Amphotericin B was provided by Squibb-Heyden.

Results

In order to study the band 3 mediated phosphate transport across the erythrocyte membrane, the effects of chloride and sulfate and the effects of competitive and noncompetitive reversible anion transport inhibitors on the phosphate self-exchange flux have been investigated. Chloride and sulfate are substrate-anions of different charge which should interfere with the binding of phosphate to the band 3 substrate site and the band 3 modifier site. Salicylate and DNDS (4,4′-dinitro-2,2′-stilbene disulfonic acid; K-salt) are competitive inhibitors of the chloride and of the sulfate transport and bind preferentially to the band 3 substrate site (Cabantchik & Rothstein, 1972, 1974; Cabantchik et al., 1978; Fröhlich, 1982; K.F. Schnell, *unpublished results*). Phlorhizin is an electroneutral and dipyridamole is a chloride-dependent, cationic anion transport inhibitor. Phlorhizin and dipyridamole elicit a noncompetitive or a mixed-type inhibition of the chloride and the sulfate transport and are supposed to bind to band 3 inhibitor sites in the vicinity of the band 3 substrate site. In contrast to dipyridamole, the inhibitors, DNDS, salicylate and phlorhizin are independent of chloride. The structure of the anion transport inhibitors is shown in Fig. 1.

As outlined already in Materials and Methods,

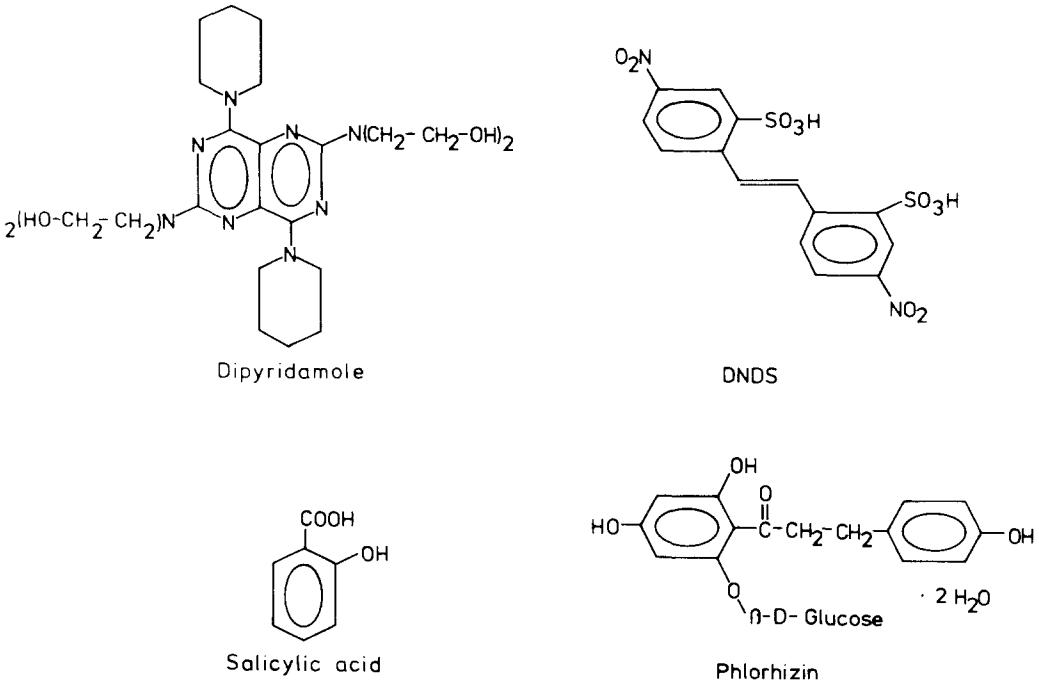

Fig. 1. Structure of the anion transport inhibitors, DNDS (4,4'-dinitro-2,2'-stilbene disulfonic acid, K-salt), salicylate, phlorhizin and dipyridamole

the phosphate self-exchange fluxes in resealed erythrocyte ghosts and in amphotericin B permeabilized erythrocytes were determined by measuring the rate of the ^{32}P-phosphate efflux and the intracellular phosphate. At self-exchange conditions, intracellular and extracellular phosphate except for the tracer are at equilibrium. Resealed erythrocyte ghosts are depleted of hemoglobin and are particularly suited to investigate the concentration dependence of the phosphate self-exchange flux at low phosphate concentrations. Throughout hemolysis, intracellular phosphate can be precisely adjusted to the required concentration. In erythrocyte ghosts, phosphate concentrations of 1–250 mM have been employed. Both the intracellular and the extracellular solutions were supplemented with 40 mM K-citrate and sucrose for isosmotic substitution. In erythrocyte ghosts, the intracellular phosphate concentration is always equal to the extracellular phosphate concentration and the equilibrium distribution of phosphate and of chloride is close to unity (Table 4). In amphothericin B (5.5 μM) permeabilized erythrocytes, phosphate concentrations of 10–400 mM have been used. To counterbalance the osmotic pressure of hemoglobin, the extracellular phosphate solutions were supplemented with 30 mM sucrose. In permeabilized erythrocytes, the equilibrium distribution of phosphate, of chloride and of sulfate (*not shown*) follows a Donnan equilibrium. As shown in Table 4, the ratios of $[P]_i/[P]_e$ and $[Cl]_i/[Cl]_e$ decrease as the concentration of extracellular phosphate is elevated. A close correlation between $\sqrt{[P]_i/[P]_e}$ and $[Cl]_i/[Cl]_e$ has been observed which indicates that phosphate behaves like a divalent anion. The volume of erythrocyte ghosts from double isotonic solutions amounts to 0.49 ± 0.03 ml/g cells wet weight and is smaller than the volume of erythrocyte ghosts from isotonic phosphate solutions which amounts to 0.65 ± 0.03 ml/g cells wet weight (Schnell & Besl, 1984), but no statistical significant differences of the phosphate self-exchange fluxes between erythrocyte ghosts from isotonic and erythrocyte ghosts from double isotonic solutions have been observed. The volume of permeabilized red cells amounts to 0.67 ± 0.03 ml/g cells wet weight and exhibits a slight decrease at phosphate concentrations of greater than 200 mM.

The effect of chloride and of sulfate on the concentration dependence of the phosphate self-exchange flux in resealed erythrocyte ghosts has been studied. The unidirectional phosphate flux in the presence of chloride is shown in Fig. 2. The flux/concentration curves exhibit saturation kinetics with an S-shaped concentration dependence at low phos-

Table 4. Equilibrium distribution of phosphate and of chloride in erythrocyte ghosts and in permeabilized erythrocytes[a]

Erythrocyte ghosts 40 mM K-citrate; pH 7.2, 25°C				
$[P]_e$ mM	$[P]_i$ mM	$[P]_i/[P]_e$	$\sqrt{[P]_i/[P]_e}$	$[Cl]_i/[Cl]_e$
1.0	0.98 ± 0.06	0.98 ± 0.06	0.99	1.06 ± 0.03
2.5	2.54 ± 0.20	1.02 ± 0.08	1.01	1.04 ± 0.06
5.0	4.89 ± 0.39	0.98 ± 0.08	0.99	1.01 ± 0.04
10.0	10.6 ± 0.80	1.06 ± 0.08	1.02	1.03 ± 0.03
25.0	26.5 ± 2.20	1.06 ± 0.08	1.03	1.04 ± 0.03
50.0	49.8 ± 2.22	0.99 ± 0.03	0.99	0.98 ± 0.05
75.0	74.2 ± 3.20	0.99 ± 0.04	0.98	1.02 ± 0.03
100	22.1 ± 3.30	0.99 ± 0.03	0.99	1.01 ± 0.04
150	149.9 ± 5.02	0.99 ± 0.03	0.99	—
200	200.5 ± 4.50	1.01 ± 0.02	1.00	—
250	250.1 ± 6.52	1.00 ± 0.03	1.00	—
Permeabilized erythrocytes 5.5 μM amphotericin B, 30 mM sucrose; pH 7.2, 25°C				
$[P]_e$ mM	$[P]_i$ mM	$[P]_i/[P]_e$	$\sqrt{[P]_i/[P]_e}$	$[Cl]_i/[Cl]_e$
10	12.8 ± 1.52	1.28 ± 0.15	1.13	1.12 ± 0.06
25	27.8 ± 1.46	1.11 ± 0.06	1.05	1.03 ± 0.07
50	49.0 ± 1.54	0.98 ± 0.09	0.99	0.92 ± 0.05
75	66.8 ± 2.12	0.89 ± 0.06	0.94	0.89 ± 0.03
100	84.6 ± 2.45	0.84 ± 0.04	0.92	0.87 ± 0.05
150	117.5 ± 3.75	0.78 ± 0.03	0.88	0.82 ± 0.07
200	156.5 ± 4.72	0.78 ± 0.04	0.86	0.84 ± 0.06
250	183.5 ± 6.15	0.73 ± 0.02	0.85	0.83 ± 0.03
300	210.9 ± 8.64	0.70 ± 0.03	0.84	0.84 ± 0.08
400	264.3 ± 7.42	0.66 ± 0.03	0.81	0.82 ± 0.06

[a] $[P]_i$, $[P]_e$ and $[Cl]_i$, $[Cl]_e$ are the intracellular and the extracellular concentrations of phosphate and of chloride. The experiments were carried out with 10% (wt/vol) suspensions of erythrocyte ghosts or of permeabilized erythrocytes. pH and temperature are indicated in the Table. The incubation solutions were labeled with either ^{32}P-phosphate and D(1-^{3}H)-glucose or with ^{36}Cl-chloride and D(1-^{3}H)-glucose. In erythrocyte ghosts, the phosphate solutions were supplemented with 40 mM K-citrate for the resealing of the ghosts and with different concentrations of sucrose for isosmotic substitution up to 660 mosM. In permeabilized red cells, the phosphate solutions were supplemented with 30 mM sucrose which cancels out the osmotic pressure of hemoglobin. $[P]_i$ and $[Cl]_i$ were assessed from the ^{32}P-phosphate, the ^{36}Cl-chloride and the D(1-^{3}H)-glucose (10 mM) equilibrium distribution as outlined in Materials and Methods. 1 mM ^{36}Cl-chloride, K-salt served as a reference anion.

phate concentrations. The sigmoidicity of the flux/concentration curves is indicated by the slope of the plots of $\log(\vec{J}_P)$ *versus* log[P]. At phosphate concentrations of 1–50 mM, the slope of the double logarithmic plots ranges from 1.08–1.12 and is significantly greater than unity. Chloride and sulfate shift the plots of $\log(\vec{J}_P)$ *versus* log[P] in parallel with the control without affecting the slope of the double logarithmic plots. In resealed erythrocyte ghosts, no concentration optimum of the phosphate self-exchange flux has been observed and at 250 mM phosphate, the flux/concentration curves are far from saturation. Trial runs with phosphate concentrations up to 600 mM and K-citrate or sucrose substitution have been performed, but also at these conditions no self-inhibition of the unidirectional phosphate flux in erythrocyte ghosts has been found. The Lineweaver-Burk plots of $1/\vec{J}_P$ *versus* 1/[P] and the Woolf-Augustinsson-Hofstee plots of $\vec{J}$ *versus* $\vec{J}_P/[P]$ (*not shown*) for the concentration dependence of the phosphate self-exchange flux are always curved. For phosphate concentrations of about 25–200 mM, the Lineweaver-Burk plots are linear, but at phosphate concentrations of smaller than 25 mM, the Lineweaver-Burk plots are curved. The Lineweaver-Burk plots for low phosphate concen-

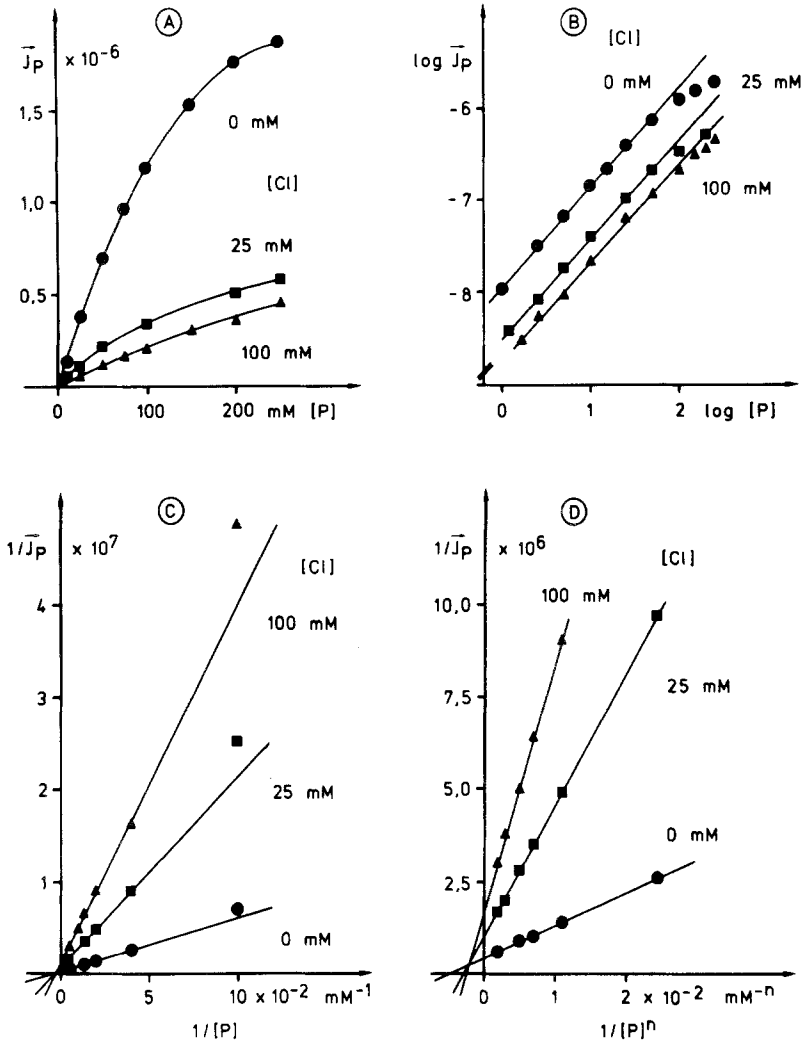

Fig. 2. The effect of chloride on the concentration dependence of the phosphate self-exchange flux in resealed erythrocyte ghosts. The experiments were carried out with 10% (wt/vol) suspensions of resealed erythrocyte ghosts, 25°C, pH 7.2. (*A*) Flux/concentration curves. (*B*) Plots of $\log(\vec{J}_P)$ *versus* log[P]. (*C*) Lineweaver-Burk plot. (*D*) Double reciprocal Hill plot. The concentration of chloride is indicated in the figure. $\vec{J}_P$ (mol/(min · g cells)) is the unidirectional phosphate flux, [P] mM is the phosphate concentration and n is the apparent Hill coefficient. $n = 1.15$

trations, intersect below the origin and yield negative phosphate half-saturation constants and negative maximal phosphate self-exchange fluxes which disprove simple saturation kinetics. Corresponding deviations from linearity have been observed in the Woolf-Augustinsson-Hofstee plots.

By contrast, the flux/concentration curves of the phosphate self-exchange flux in erythrocyte ghosts can easily be fitted to the double reciprocal Hill plot or to the Hill-Hofstee plot (*not shown*). The double reciprocal Hill plots of $1/\vec{J}_P$ *versus* $1/[P]^n$ at different fixed concentrations of chloride or sulfate and the corresponding Hill-Hofstee plots of $\vec{J}_P$ *versus* $\vec{J}_P/[P]^n$ are linear and provide apparent Hill coefficients of greater than unity which are suggestive for a positive cooperativity of the phosphate self-exchange flux. Families of double reciprocal Hill plots at different fixed chloride or sulfate (*not shown*) concentrations have a common intersection point the left of the $1/\vec{J}_P$-axis and above the $1/[P]^n$-axis. The respective Hill-Hofstee plots exhibit a decrease in slope and in the $\vec{J}_P$-axis intercept as the chloride or the sulfate concentrations are elevated.

The concentration dependence of the phosphate self-exchange flux in amphotericin B permeabilized red blood cells is different from the concentration dependence of the phosphate self-exchange flux in erythrocyte ghosts (Fig. 3). In permeabilized erythrocytes, the equilibrium distribution of phosphate and of the inhibiting anions, chloride and sulfate, follows a Donnan equilibrium. At phosphate concentrations of 10–50 mM, the flux/concentration curves display a sigmoidal concentration responsiveness as indicated by the slope of the plots of $\log(\vec{J}_P)$ *versus* log[P] which always is greater than unity. In contrast to erythrocyte ghosts, the flux/concentration curves in permeabilized erythrocytes pass through a concentration optimum at about 150–200 mM phosphate

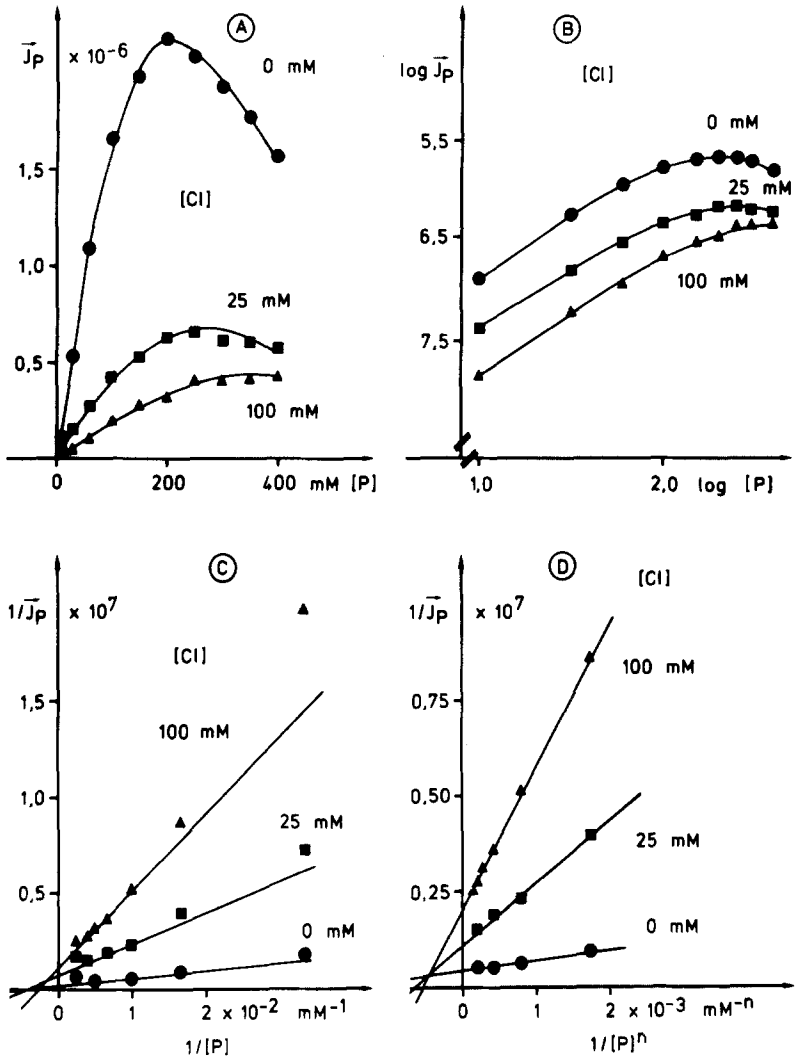

Fig. 3. The effect of chloride on the concentration dependence of the phosphate self-exchange flux in permeabilized erythrocytes. The experiments were carried out with 10% (wt/vol) suspensions of permeabilized cells, pH 7.2, 25°C, 5.5 μM amphotericin B. (*A*) Flux/concentration curve. (*B*) Plot of log ($\vec{J}_P$) *versus* log[P]. (*C*) Lineweaver-Burk plot. (*D*) Double-reciprocal Hill plot. The chloride concentrations are indicated in the figures. $\vec{J}_P$ (mol/(min · g cells)) is the unidirectional phosphate flux, [P] mM is the phosphate concentration and n is the apparent Hill coefficient. n = 1.42–1.65

and at phosphate concentrations of greater than 200 mM, self-inhibition becomes predominant. Chloride and sulfate (*not shown*) inhibit the phosphate self-exchange flux, reduce self-inhibition of the phosphate flux and shift the flux optimum towards higher phosphate concentrations. At 100 mM chloride or sulfate, the flux optimum of the phosphate self-exchange flux disappears. The Lineweaver-Burk and the Woolf-Augustinsson-Hofstee plots for the ascending branches of the flux/concentration curves show similar features as in resealed erythrocyte ghosts. Both the Lineweaver-Burk and the Woolf-Augustinsson-Hofstee plots are curved. For low phosphate concentrations, the Lineweaver-Burk and the Woolf-Augustinsson-Hofstee plots give negative phosphate half-saturation constants and negative maximal phosphate self-exchange fluxes which rule out simple saturation kinetics. With regard to the Lineweaver-Burk plot, the self-inhibition of phosphate flux is indicated by an increase of $1/\vec{J}_P$ as 1/[P] approaches zero, but the self-inhibition cannot account for intersection points below the origin. The Woolf-Augustinsson-Hofstee plots in the presence of self-inhibition show a decrease of the $\vec{J}_P$ at high phosphate concentrations when $\vec{J}_P/[P]$ goes to zero.

Conversely, the ascending branches of the flux/concentration curves can be fitted to the double-reciprocal Hill plot of $1/\vec{J}_P$ *versus* $1/[P]^n$ or to the Hill-Hofstee plot of $\vec{J}_P$ *versus* $\vec{J}_P/[P]^n$ (*not shown*) with n being the apparent Hill coefficient for the phosphate self-exchange flux. Both plots are linear and provide apparent Hill coefficients of greater than unity which are indicative to sigmoidal flux/concentration curves. The double-reciprocal Hill plots for different fixed concentrations of chloride or sulfate intersect to the left of the $1/\vec{J}_P$-axis and above the $1/[P]^n$-axis. Correspondingly, the slope of the Hill-Hofstee plots is enhanced and the $\vec{J}_P$-axis intercept is reduced as the concentrations of chloride or of sulfate are elevated. Self-inhibition of the phosphate flux is indi-

Table 5. The effect of chloride and of sulfate upon the concentration dependence of the phosphate self-exchange flux in erythrocyte ghosts and in amphotericin B permeabilized erythrocytes[a]

Resealed erythrocyte ghosts Phosphate: 1–250 mM, 40 mM K-citrate; 25°C, pH 7.2				
$[I]$ mM	n —	$K_{P(app)}$ mM		$\vec{J}_{max(app/P)}$ mol/(min · g cells)
		Chloride		
0	1.15 ± 0.02	120 ± 12		$(2.526 \pm 0.186) \times 10^{-6}$
25	1.15 ± 0.04	132 ± 9		$(1.062 \pm 0.098) \times 10^{-6}$
100	1.16 ± 0.03	156 ± 14		$(5.135 \pm 0.462) \times 10^{-7}$
		Sulfate		
0	1.15 ± 0.02	125 ± 15		$(2.682 \pm 0.256) \times 10^{-6}$
25	1.14 ± 0.02	148 ± 12		$(1.824 \pm 0.225) \times 10^{-6}$
100	1.18 ± 0.05	196 ± 21		$(1.436 \pm 0.108) \times 10^{-6}$
Permeabilized erythrocytes Phosphate: 10–400 mM, 30 mM sucrose, 5.5 μM amphotericin B; pH 7.2, 25°C				
$[I]$ mM	n —	$K_{P(app)}$ mM	$K_{iP(app)}$ mM	$\vec{J}_{max(app/P)}$ mol/(min · g cells)
		Chloride		
0	1.65 ± 0.05	75 ± 5	(552)	$(2.519 \pm 0.342) \times 10^{-6}$
25	1.46 ± 0.02	82 ± 4	(762)	$(7.373 \pm 0.628) \times 10^{-7}$
100	1.42 ± 0.03	152 ± 14	—	$(4.796 \pm 0.352) \times 10^{-7}$
		Sulfate		
0	1.55 ± 0.06	72 ± 6	(530)	$(2.608 \pm 0.097) \times 10^{-6}$
50	1.52 ± 0.03	110 ± 12	(620)	$(1.884 \pm 0.236) \times 10^{-6}$
100	1.27 ± 0.04	122 ± 8	—	$(1.092 \pm 0.087) \times 10^{-6}$

[a] The experiments were carried out with 10% (wt/vol) suspensions of erythrocyte ghosts or amphotericin B (5.5 μM) permeabilized red cells. pH, temperature, chloride and sulfate are indicated in the Table. The apparent Hill coefficients, n, the apparent phosphate half-saturation constants, $K_{P(app)}$, and the apparent maximal unidirectional phosphate fluxes, $\vec{J}_{max(app/P)}$, were obtained by fitting the flux/concentration curves to the double reciprocal Hill plot and to the Hill-Hofstee plot. The correction coefficients for the fits were always better than 0.997. $[I]$ is the concentration of the inhibiting anion.

cated in the double reciprocal Hill plot by a sharp increase of $1/\vec{J}_P$ at low $1/[P]^n$ and by a sharp decrease of $\vec{J}_P$ at low $\vec{J}_P/[P]^n$ in the Hill-Hofstee plot.

The apparent phosphate half-saturation constants, the apparent maximal phosphate self-exchange fluxes and the apparent Hill coefficients for the phosphate self-exchange fluxes are summarized in Table 5. In erythrocyte ghosts, the apparent phosphate half-saturation constant is approximately 125 mM, whereas in amphothericin B permeabilized erythrocytes, the apparent phosphate half-saturation constant is about 75 mM. The apparent Hill coefficients in permeabilized red cells and in erythrocyte ghosts amount to approximately 1.60 and 1.15, respectively. In permeabilized cells, the Hill coefficients are slightly reduced by chloride and by sulfate while in erythrocyte ghosts, the apparent Hill coefficients do not respond to chloride or to sulfate. The Hill coefficients indicate a positive cooperativity of phosphate self-exchange flux which can result from a cooperativity of the phosphate binding at the membrane surfaces or from a cooperativity of phosphate translocation across the erythrocyte membrane. Chloride and sulfate elicit a mixed-type inhibition of the phosphate self-exchange flux. Both of these anions increase the apparent half-saturation constants and reduce the apparent maximal self-exchange fluxes of phosphate.

Furthermore, the inhibition of the phosphate self-exchange flux by chloride and sulfate in resealed erythrocyte ghosts and in amphotericin B permeabilized erythrocytes has been studied. The dose-response curves for the phosphate self-exchange flux have been measured at a fixed phosphate concentra-

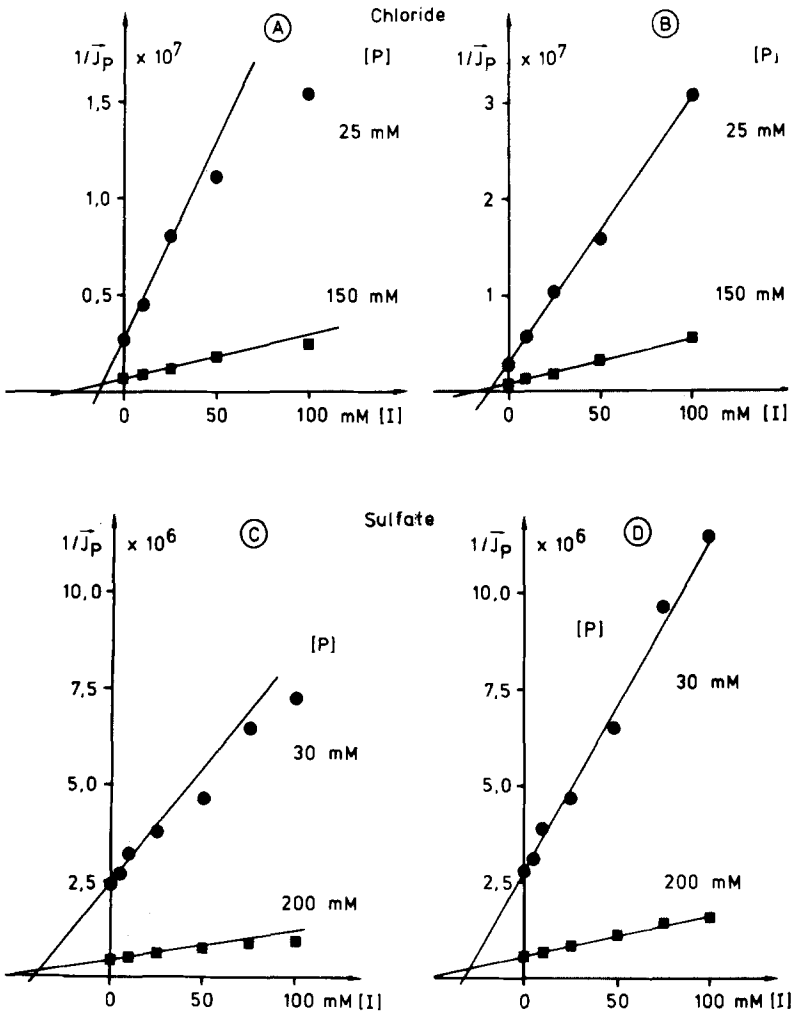

Fig. 4. The inhibition of the phosphate flux by chloride and by sulfate in resealed erythrocyte ghosts. The experiments were carried out with 10% suspensions of resealed erythrocyte ghosts, pH 7.2, 25°C. (*A,C*) Dixon plots for chloride and sulfate. (*B,D*) Dixon plots for chloride and sulfate upon subtraction of a 3–5% residual flux. Phosphate concentrations [P] are indicated in the figure. $\vec{J}_P$ [mol/(min · g cells)] is the unidirectional phosphate flux and [*I*] mM is the concentration of chloride or sulfate, respectively

tion and at increasing concentrations of the inhibiting anions. In erythrocyte ghosts, the intracellular concentrations of phosphate, chloride and sulfate are equal to the extracellular concentrations, whereas in permeabilized red cells penetrating anions distribute according to a Donnan equilibrium. The Dixon plots for chloride and for sulfate in resealed erythrocyte ghosts are shown in Fig. 4. The Dixon plots for chloride and for sulfate are hyperbolic and get linear upon subtraction of an appropriate residual phosphate self-exchange flux. The Dixon plots in erythrocyte ghosts intersect above the [*I*]-axis and indicate a competitive inhibition of the phosphate self-exchange flux by chloride and by sulfate. The Hill-Dixon plots and the plots of $\log(i/(i_{max}-i))$ *versus* $\log[I]$ (*not shown*) give apparent Hill coefficients of approximately 1.0 for chloride and for sulfate binding in erythrocyte ghosts. By contrast, the Dixon plots for chloride and for sulfate in permeabilized erythrocytes are parabolic. The Hill-Dixon plots for chloride and for sulfate are linear and give apparent Hill coefficients of approximately 1.15 for chloride and of about 1.25 for sulfate. The Hill-Dixon plots for chloride and for sulfate intersect below the $[I]^m$-axis and point towards a mixed-type inhibition of the phosphate self-exchange flux by chloride and by sulfate (*not shown*). In permeabilized cells, the increase of extracellular chloride and of extracellular sulfate elicits a decrease of the intracellular phosphate concentration and consequently, the phosphate self-exchange fluxes at high chloride or sulfate concentrations may be too low. Possibly, this effect can account for the parabolic Dixon plots in permeabilized red cells, but it cannot rule out differences of chloride and sulfate binding between erythrocyte ghosts and permeabilized erythrocytes. The apparent inhibition constants and the apparent Hill coefficients for chloride and for sulfate in erythrocyte ghosts and in permeabilized red blood cells are listed in Table 6.

The concentration dependence of the phosphate self-exchange flux in the presence of the anionic inhibitors, DNDS and salicylate (*not shown*), exhibits the same features as the concentration respon-

Table 6. Inhibition of the phosphate self-exchange flux by chloride and by sulfate in erythrocyte ghosts and permeabilized erythrocytes[a]

Resealed erythrocyte ghosts 40 mM K-citrate; 25°C, pH 7.2				
[P] mM	[*I*] mM	*m* —	$K_{i(app)}$ mM	$\vec{J}_{P(o)}$ mol/(min · g cells)
		Chloride		
25	0–100	1.02 ± 0.03	12 ± 3	(3.802 ± 0.229) × 10^{-7}
150	0–100	0.98 ± 0.02	21 ± 5	(1.547 ± 0.262) × 10^{-6}
		Sulfate		
30	0–100	1.01 ± 0.02	47 ± 5	(4.124 ± 0.104) × 10^{-7}
75	0–100	0.98 ± 0.02	59 ± 4	(1.022 ± 0.098) × 10^{-6}
150	0–100	1.02 ± 0.04	122 ± 21	(1.066 ± 0.248) × 10^{-6}
Permeabilized erythrocytes 5.5 μM amphotericin B, 30 mM sucrose; pH 7.2, 25°C				
[P] mM	[*I*] mM	*m* —	$K_{i(app)}$ mM	$\vec{J}_{P(o)}$ mol/(min · g cells)
		Chloride		
10	0–100	1.25 ± 0.04	49 ± 6	(1.142 ± 0.087) × 10^{-7}
100	0–100	1.26 ± 0.03	33 ± 7	(1.416 ± 0.181) × 10^{-6}
		Sulfate		
10	0–100	1.30 ± 0.02	69 ± 5	(1.247 ± 0.204) × 10^{-7}
100	0–100	1.30 ± 0.02	48 ± 6	(1.734 ± 0.236) × 10^{-6}

[a] The experiments were carried out with 10% (wt/vol) suspensions of erythrocyte ghosts or of permeabilized erythrocytes. pH, temperature and amphotericin B concentration are indicated in the Table. [P] is the phosphate concentration, *m* the apparent Hill coefficient for the inhibitor, $\vec{J}_{P(i)}$ and $\vec{J}_{P(o)}$ are the unidirectional phosphate fluxes in the presence and the absence of inhibitors, and $K_{i(app)}$ is the apparent inhibition constant of chloride and sulfate from the Hill-Dixon plot.

siveness of the phosphate self-exchange flux in the presence of chloride and of sulfate (Fig. 5). The Lineweaver-Burk and the Woolf-Augustinsson-Hofstee plots are curved and extrapolation from low phosphate concentrations give negative phosphate half-saturation constants and negative maximal phosphate fluxes and rule out saturation kinetics. The sigmoidicity of the flux/concentration curves is indicated by the slope of the double logarithmic plots of $\log(\vec{J}_P)$ *versus* log[P] which is always greater than unity. DNDS and salicylate inhibit the unidirectional phosphate flux and shift the double logarithmic plots in parallel with control. The double reciprocal Hill plots and the Hill-Hofstee plots (*not shown*) for DNDS and salicylate are linear and give apparent Hill coefficients of greater than unity. The double reciprocal Hill plots have a common intersection point to the left of the $1/\vec{J}_P$-axis and above the $1/[P]^n$-axis and display the features of a mixed-type inhibition. The apparent Hill coefficients are insensitive to DNDS and to salicylate and indicate that the cooperativity of the phosphate self-exchange flux does not respond to these anion transport inhibitors.

By contrast, the nonionic anion transport inhibitor, phlorhizin, and the cationic anion transport inhibitor, dipyridamole, modify the concentration dependence of the phosphate self-exchange flux in resealed erythrocyte ghosts. Phlorhizin decreases the slope of the log $(\vec{J}_P)$ *versus* log[P] plots at 2 mM phlorhizin, the Lineweaver-Burk plot for the phosphate self-exchange flux in resealed ghosts becomes linear (Fig. 6). Correspondingly, the apparent Hill coefficient for the phosphate self-exchange flux is reduced from about 1.15–0.95. The double reciprocal Hill plots of the flux/concentration curves for phlorhizin intersect upon the $1/[P]^n$-axis and provide strong evidence for a noncompetitive inhibition of the phosphate transport by phlorhizin. The chloride-dependent, cationic inhibitor dipyridamole elicits a mixed-type inhibition of the phosphate self-exchange flux (*not shown*), but in contrast to DNDS and salicylate, the apparent Hill coefficients are re-

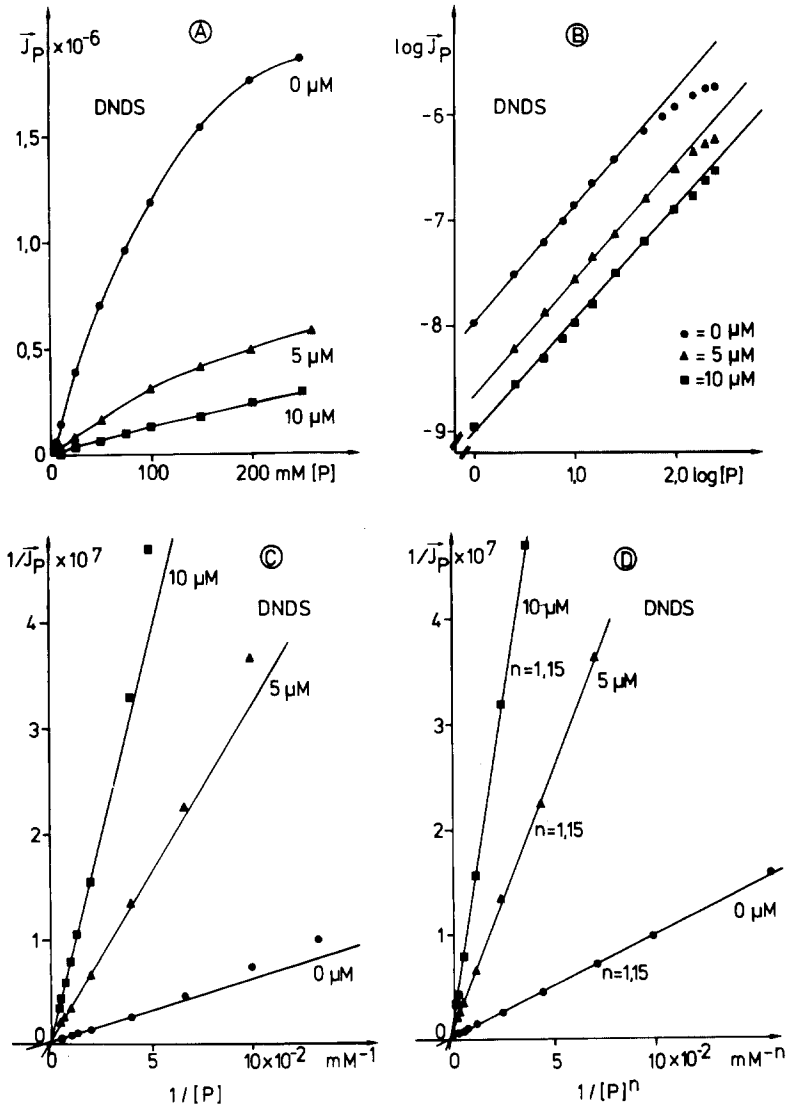

Fig. 5. The effect of DNDS on the concentration dependence of the phosphate self-exchange flux in resealed erythrocyte ghosts. The experiments were carried out with 10% suspensions in resealed erythrocyte ghosts, pH 7.2, 25°C. (*A*) Flux/concentration curve. (*B*) Plot of $\log(\vec{J}_P)$ *versus* log[P]. (*C*) Lineweaver-Burk plot. (*D*) Double reciprocal Hill plot. DNDS is indicated in the figure. $\vec{J}_P$ [mol/(min · g cells)] is the unidirectional phosphate flux, [P] mM the phosphate concentration and n the apparent Hill coefficient. n = 1.15

duced by dipyridamole. The apparent half-saturation constants, the apparent maximal unidirectional phosphate fluxes and the apparent Hill coefficients are summarized in Table 7.

In order to get additional information about the mechanism of phosphate transport, the inhibition of the phosphate self-exchange flux by the anion transport inhibitors has been studied. The inhibition of the phosphate self-exchange flux by the anion transport inhibitors is incomplete and approaches asymptotically a limiting value. The dose-response curves of DNDS and of dipyridamole are shown in Fig. 7. The inhibitor-insensitive residual flux is indicated by dashed lines. Similar results have been obtained with salicylate and phlorhizin (*not shown*). As already mentioned in Materials and Methods, the dose-response curves were analyzed by means of the Hill-Dixon plot of $1/\vec{J}_P$ *versus* $[I]^m$, with m being the apparent Hill coefficient for inhibitor binding (Table 2). The inhibitor-insensitive residual flux is indicated by hyperbolic Dixon plots which become linear upon subtraction of an appropriate residual flux. In this plot, the residual phosphate flux is interrelated with the apparent Hill coefficient and the subtraction of a wrong residual flux modifies the apparent Hill coefficient for inhibitor binding. More precisely, the dose-response curves can be analyzed by means of the double-logarithmic plot of $\log(i/(i_{max}-i))$ *versus* $\log[I]$. In these plots, i and i_{max} are the fractional inhibition and the maximal fractional inhibition of the phosphate self-exchange flux and $[I]$ is the inhibitor concentration. In these plots, self inhibition of the phosphate self-exchange flux cancels out and the apparent Hill coefficient, m, for inhibitor binding can be assessed independent of i_{max}. The slope of the plot is m and at $\log(i/(i_{max}$ –

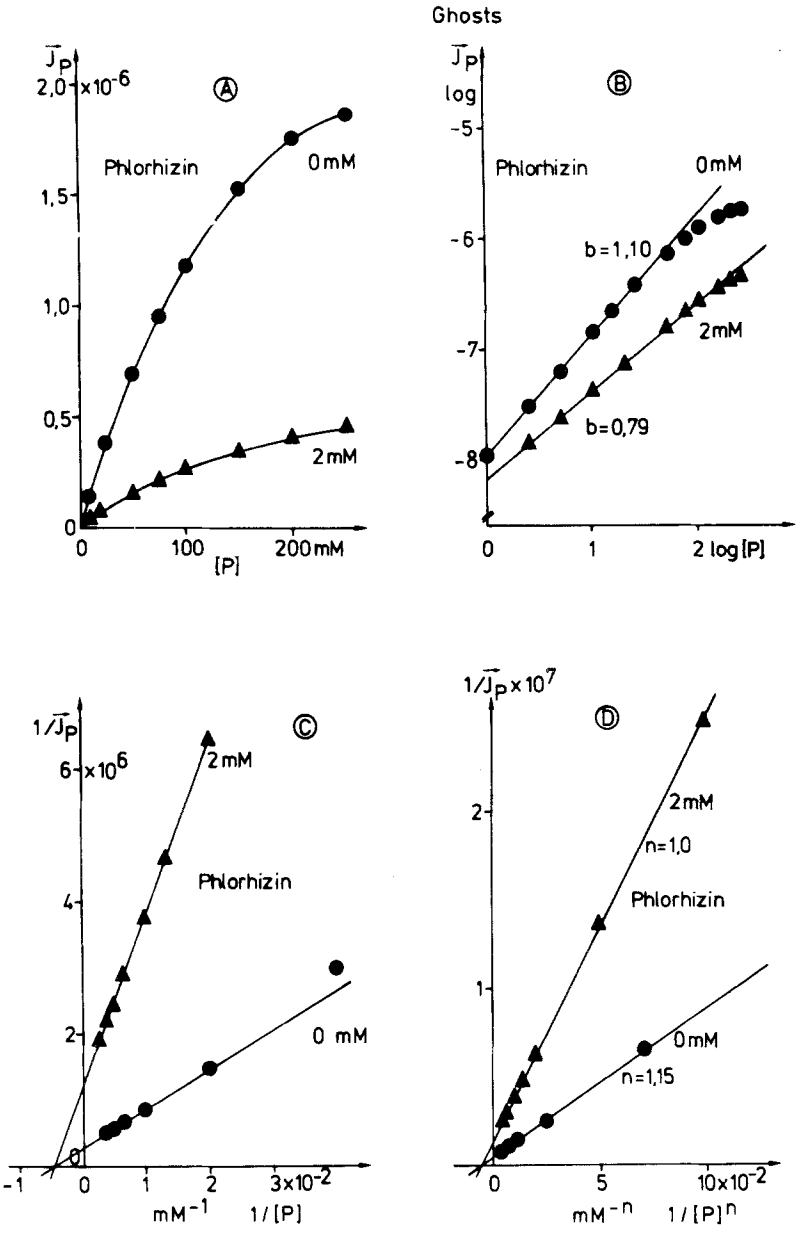

Fig. 6. The effect of phlorhizin on the concentration dependence of the phosphate self-exchange flux in resealed erythrocyte ghosts. The experiments carried out with 10% suspensions, pH 7.2, 25°C. (*A*) Flux/concentration curve. (*B*) Plots of $\log(\vec{J}_P)$ *versus* log[P]. (*C*) Lineweaver-Burk plot. (*D*) Double reciprocal Hill plot. Phlorhizin is indicated in the figure

$i)) = 0$ the corresponding log $[I]$ value is $\log[I]_{0.5}$. For details *see* Table 3.

The plots of $\log(i/(i_{max}-i))$ *versus* $\log[I]$ for DNDS and for dipyridamole are shown in Fig. 8. The slope of the plots is close to 1.0 and indicate a noncooperative inhibition of the phosphate flux by DNDS or dipyridamole. The inhibitor-insensitive residual phosphate flux in resealed erythrocyte ghosts, is always higher than in intact erythrocytes. In intact red blood cells, the inhibitor-insensitive residual phosphate flux amounts to about 1% of control while in erythrocyte ghosts the inhibitor-insensitive residual phosphate flux amounts to 3–7% of control. This corresponds to a maximal fractional inhibition of 99% in intact erythrocytes and of 93–97% in erythrocyte ghosts. The inhibitor-insensitive residual phosphate flux in resealed ghosts and in intact erythrocytes indicates an incomplete inhibition of the phosphate transport by the anion transport inhibitors. The apparent Hill coefficients for the inhibitors were obtained from the slope of the plots of $\log(i/(i_{max}-i))$ *versus* $\log[I]$ and are in the range of 0.95–1.0. These results indicate a linear relation between inhibitor binding and inhibition of the phosphate self-exchange flux. The apparent Hill coefficients for inhibitor binding, the apparent inhibition constants, the apparent maximal unidirectional phosphate flux and the maximum inhibition of the phosphate flux are listed in Table 8.

In order to diagnose the pattern of inhibition,

Table 7. The effect of the anion transport inhibitors DNDS, salicylate, phlorhizin and dipyridamole upon the concentration dependence of the phosphate self-exchange flux in resealed erythrocyte ghosts[a]

Resealed erythrocyte ghosts Phosphate: 1–250 mM, 40 mM K-citrate; 25°C, pH 7.2			
$[I]$	n —	$K_{P(app)}$ mM	$\vec{J}_{max(app/P)}$ mol/(min · g cells)
0	1.14 ± 0.01	140 ± 8	(2.629 ± 0.324) × 10^{-6}
DNDS (4,4'-dinitro-2,2'-stilbenedisulfonic acid)			
5 μM	1.15 ± 0.03	247 ± 25	(1.428 ± 0.213) × 10^{-6}
10 μM	1.16 ± 0.05	486 ± 50	(8.953 ± 0.786) × 10^{-7}
Salicylate			
1.0 mM	1.17 ± 0.03	295 ± 25	(1.429 ± 0.242) × 10^{-6}
2.5 mM	1.12 ± 0.04	376 ± 42	(8.266 ± 0.722) × 10^{-7}
Phlorhizin			
2.0 mM	0.98 ± 0.04	150 ± 26	(6.995 ± 0.248) × 10^{-7}
4.0 mM	0.96 ± 0.03	145 ± 21	(2.142 ± 0.242) × 10^{-7}
Dipyridamole (20 mM KCl)			
0 μM	1.15 ± 0.02	150 ± 15	(1.667 ± 0.089) × 10^{-6}
5 μM	1.10 ± 0.03	175 ± 25	(4.389 ± 0.136) × 10^{-7}
10 μM	1.02 ± 0.04	476 ± 42	(3.572 ± 0.095) × 10^{-7}

[a] The experiments were carried out with 10% (wt/vol) suspensions of resealed erythrocyte ghosts. pH and temperature are indicated in the Table. n is the apparent Hill coefficient for phosphate, $K_{P(app)}$ is the apparent phosphate half-saturation constant and $\vec{J}_{max(app/P)}$ is the apparent maximal phosphate flux from the double reciprocal Hill plot or the Hill-Hofstee plot.

the Dixon plots have been employed. Because of the inhibitor-insensitive residual flux, the Dixon plots for DNDS, salicylate, phlorhizin and dipyridamole in resealed erythrocyte ghosts were curved, but they get linear upon the subtraction of a suitable residual flux. The extrapolation from the linear parts of the Dixon plots and the Dixon plots after subtraction of the inhibitor-insensitive residual flux show the same patterns of inhibition. Surprisingly, the Dixon plots for the inhibitors, DNDS and salicylate, and for the inhibitors, phlorhizin and dipyridamole, all intersect on the $[I]$-axis and point to a noncompetitive inhibition of the phosphate transport by the anion transport inhibitors (Fig. 9).

The results of our studies show appreciable difference between the phosphate self-exchange flux in erythrocytes, in amphothericin B permeabilized erythrocytes and in resealed erythrocyte ghosts. The concentration dependence of the phosphate self-exchange flux exhibits a positive cooperativity in erythrocyte ghosts and in permeabilized erythrocytes, but as indicated by the apparent Hill coefficients, sigmoidicity of the flux/concentration curves in permeabilized cells is more pronounced than in resealed erythrocyte ghosts. In contrast to permeabilized red cells, no self-inhibition of the phosphate flux has been observed in erythrocyte ghosts. The double reciprocal Hill plots for the phosphate self-exchange flux in the presence of chloride, sulfate, DNDS, salicylate and dipyridamole indicate a mixed-type inhibition of the phosphate self-exchange flux. By contrast, the Hill-Dixon plots indicate a competitive inhibition of the phosphate self-exchange flux by chloride and by sulfate in erythrocyte ghosts and a mixed-type inhibition of the phosphate self-exchange flux by chloride and by sulfate in permeabilized erythrocytes. The Dixon plots for the anion transport inhibitors DNDS and salicylate, for the cationic, chloride-dependent anion transport inhibitor dipyridamole and the electroneutral anion transport inhibitor phlorhizin are linear and indicate a noncompetitive inhibition of the phosphate self-exchange flux by these inhibitors. As will be discussed below, the sigmoidicity of the flux/concentration curves and the controversial patterns of inhibition of the phosphate self-exchange flux most probably arise from the effects of ionic strength on the binding of phosphate and of inhibitors to band 3 and on the band 3 mediated translocation of phosphate across the erythrocyte membrane.

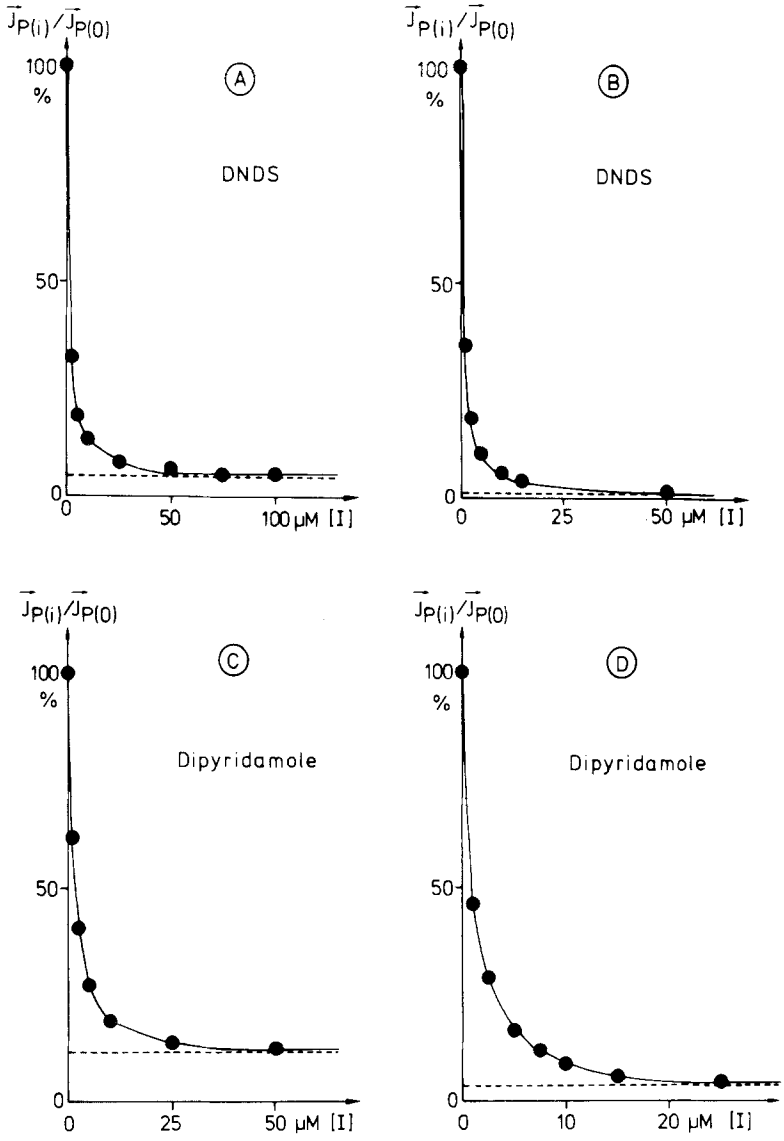

Fig. 7. The inhibition of the phosphate self-exchange flux by DNDS and dipyridamole in resealed ghosts and in intact red blood cells. The fractional flux $\vec{J}_{P(i)}/\vec{J}_{P(o)}$ is plotted *versus* the inhibitor concentration [*I*]. The experiments were carried out with 10% suspensions, pH 7.3, 25°C. The dashed lines indicate the residual flux. (*A,B*) DNDS, resealed erythrocyte ghosts and red blood cells. (*C,D*) Dipyridamole plus 20 mM KCl, resealed erythrocyte ghosts, and intact red blood cells

Discussion

As already mentioned, anion transport across the erythrocyte membrane is catalyzed by band 3, but the mechanism of the transport catalysis remains to be established. With regard to anion transport, band 3 could function as a carrier with a single substrate site which is alternately exposed to the inner or the outer membrane surface. Conversely, band 3 could function as a dielectric pore with one substrate site at the inner membrane surface and one substrate site at the outer membrane surface as proposed by Schnell (1977) and more recently by Tanford (1985). Irrespective of whether band 3 functions as a carrier or as a dielectric pore, anion transport across the erythrocyte membrane consists of three consecutive steps. For its transport across the red cell membrane, the transported anion first gets bound to the band 3 substrate site at one of the membrane surfaces. Upon binding, the substrate-anion is translocated across the erythrocyte membrane and finally, the transported anion is released at the opposite membrane surface. The translocation of a substrate-anion by a carrier transport mechanism is associated with a conformational change of the transport protein. For a dielectric pore, the substrate-anion diffuses along the pore and the conformational changes of the transport protein can be kept at a minimum. Most probably, the translocation of phosphate and of chloride are distinguished by the fact that phosphate translocation is activated by the binding of a second H^+ to the band 3 substrate site which is not required for the translocation of chloride. As known so far, there are several lysine, arginine and aspara-

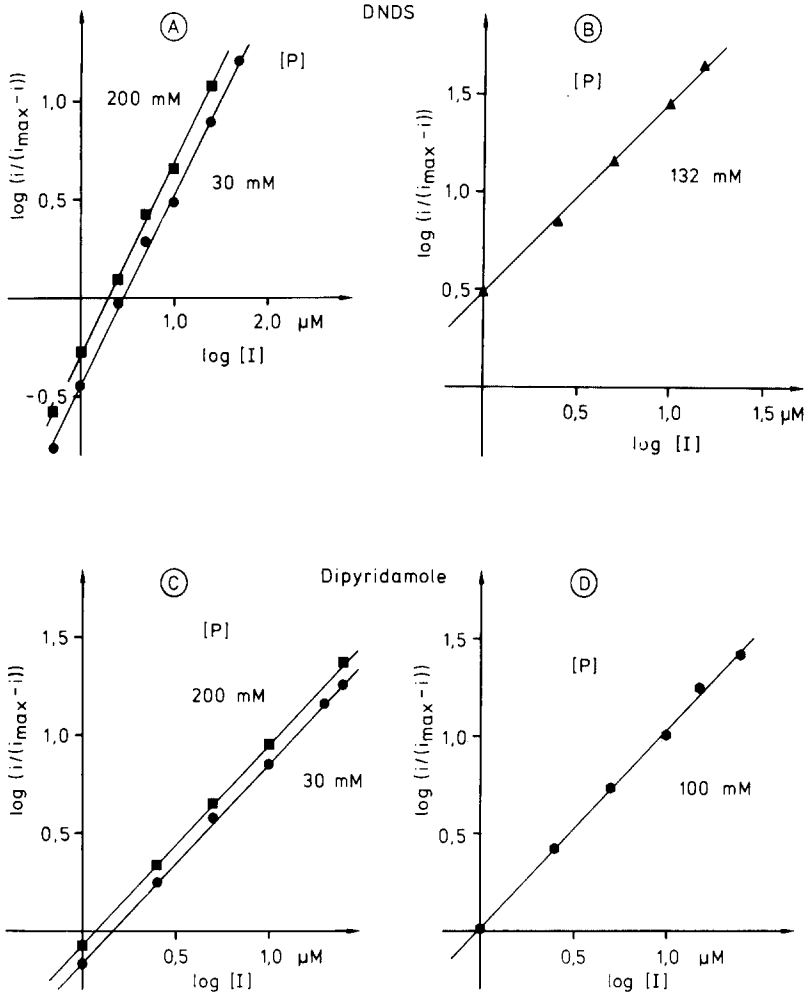

Fig. 8. Plots of $\log(i/(i_{max}-i))$ *versus* $\log[I]$ for assessing the inhibitor-insensitive residual phosphate flux and the apparent Hill coefficient of the inhibitor. The experiments were carried out with 10% suspension of resealed erythrocyte ghosts, pH 7.2, 25°C. i and i_{max} are the fractional inhibition and the maximal fractional inhibition of the flux, $[I]$ is the inhibitor concentration. The slope of the plots provides the apparent Hill coefficient for inhibitor binding

gine residues which are located at the band 3 substrate site or in its immediate vicinity. Depending on their electrical charge, these groups can either improve or inhibit the binding of phosphate to the band 3 substrate site. Substrate-anions such as chloride and sulfate or true competitive inhibitors of the anion transport should compete with phosphate for the band 3 substrate site and should elicit a competitive inhibition of phosphate transport. Conversely, noncompetitive anion transport inhibitors should bind to band 3 inhibitor sites which are distinct from the band 3 substrate site. Therefore, noncompetitive anion transport inhibitors should not interfere with phosphate binding to the band 3 substrate site, but rather they should impair phosphate translocation across the erythrocyte membrane. There is a large variety of reactions which can elicit a noncompetitive inhibition of phosphate transport. Noncompetitive inhibitors can inhibit the activation of the translocation by shielding ionizing groups, they can inhibit conformational changes of the transport protein by stabilizing a distinct conformation or they can change the energy profile of a dielectric pore and increase the height of diffusion barriers without blocking the substrate sites. For all these cases a noncompetitive inhibition of phosphate self exchange is to be expected.

Because of the sigmoidicity of the phosphate self-exchange flux, the flux/concentration curves and the dose-response curves were fitted to extended Hill equations. The Hill equation (Hill, 1910) and the extended Hill equations are empirical equations, but they offer a mathematical description for the interaction of phosphate and of different types of anion transport inhibitors with a multi-site transport system. Since the Hill equations have the same structure as the corresponding Michaelis-Menten equations, the same transformations can be made. The double reciprocal Hill plots ($1/\vec{J}_P$ *versus* $1/[P]^n$) and the Hill-Hofstee plots ($\vec{J}_P$ *versus* $\vec{J}_P/[P]^n$) provide the apparent Hill coefficient, the apparent half-saturation constant and the apparent maximal phosphate self-exchange flux. An obstacle to the analysis of the flux/concentration curves can arise from self-

Table 8. The inhibition of the phosphate self-exchange flux in resealed erythrocyte ghosts and in intact erythrocytes by the anion transport inhibitors DNDS, salicylate, phlorhizin and dipyridamole[a]

$K_{i(app)}$	$\vec{J}_{P(o)}$ mol/(min · g cells)	i_{max} %
Resealed erythrocyte ghosts Phosphate: 200 mM, 40 mM K-citrate; pH 7.2, 25°C		
	DNDS: 0–50 μM	
870 ± 120 nM	(1.445 ± 0.257) × 10^{-6}	97
	Salicylate: 0–5 mM	
656 ± 142 μM	(1.547 ± 0.096) × 10^{-6}	97
	Phlorhizin: 0–5 mM	
496 ± 64 μM	(1.789 ± 0.207) × 10^{-6}	97
	Dipyridamole: 0–50 μM, 20 mM KCl	
1.38± 0.21 μM	(9.876 ± 0.062) × 10^{-7}	94
Erythrocytes Phosphate: 132 mM, 25°C, pH 7.2		
	DNDS: 0–50 μM	
610 ± 52 nM	(1.786 ± 0.216) × 10^{-6}	<99
	Salicylate: 0–50 mM	
620 ± 125 μM	(1.626 ± 0.322) × 10^{-6}	<99
	Phlorhizin: 0–5.0 mM	
525 ± 85 μM	(1.524 ±0.256) × 10^{-6}	<99
	Dipyridamole (20 mM KCl): 0–50 μM	
1.44 ± 0.25 μM	(1.205 ± 0.132) × 10^{-6}	<98

[a] The experiments were carried out with 10% suspensions of resealed erythrocyte ghosts or of intact erythrocytes, 25°C, pH 7.2. Inhibitor concentration is indicated in the Table. The apparent Hill coefficient for the inhibitor, m, is always approximately 1.0. $K_{i(app)}$ is the apparent inhibition constant from the Hill-Dixon plots, $\vec{J}_{P(o)}$ is the phosphate flux at zero inhibitor and i_{max} is the maximal inhibition of the phosphate self-exchange flux.

inhibition of the phosphate flux. As already mentioned, a linear self-inhibition is difficult to perceive and can result in an underestimate of the phosphate half-saturation constant and of the maximum phosphate self-exchange flux and in an overestimate of the apparent Hill coefficient for phosphate. As shown in Table 1, families of double reciprocal Hill plots for a competitive and a noncompetitive inhibitor intersect on the $1/\vec{J}_P$-axis and on the $1/[P]^n$-axis. A mixed-type inhibition in the double reciprocal Hill plots is indicated by an intersection point to the left of the $1/\vec{J}_P$-axis and above the $1/[P]^n$-axis and arises from either a two-site binding of the inhibitor or from a linear self-inhibition of the flux.

The Hill-Dixon plot of $1/\vec{J}_P$ *versus* $[I]^m$ and the double logarithmic plot of $\log(i/(i_{max}-i))$ *versus* $\log[I]$ give the apparent inhibition constant, $K_{i(app)}$, the half-inhibition concentration of the inhibitor, $[I]_{0.5}$, and m, the apparent Hill coefficient for the inhibitor. For a competitive inhibitor, the Hill-Dixon plots intersect above the $[I]^m$-axis while for a noncompetitive inhibitor, the Hill-Dixon plots intersect on the $[I]^m$-axis. An inhibitor-insensitive residual phosphate flux is indicated by hyperbolic Dixon plots while a Hill coefficient of greater than unity is indicated by parabolic Dixon plots. At $m = 1$, the inhibitor-insensitive residual phosphate flux can be determined by the substraction of an appropriate residual fluxé until the Dixon plot gets linear, but for $m < 1$ or for $m > 1$, this procedure yields wrong Hill coefficients and wrong inhibition constants. Furthermore, self-inhibition of the phosphate flux shifts the intersection points of the Hill-Dixon plots towards the $[I]^m$-axis and the plots then may indicate a wrong

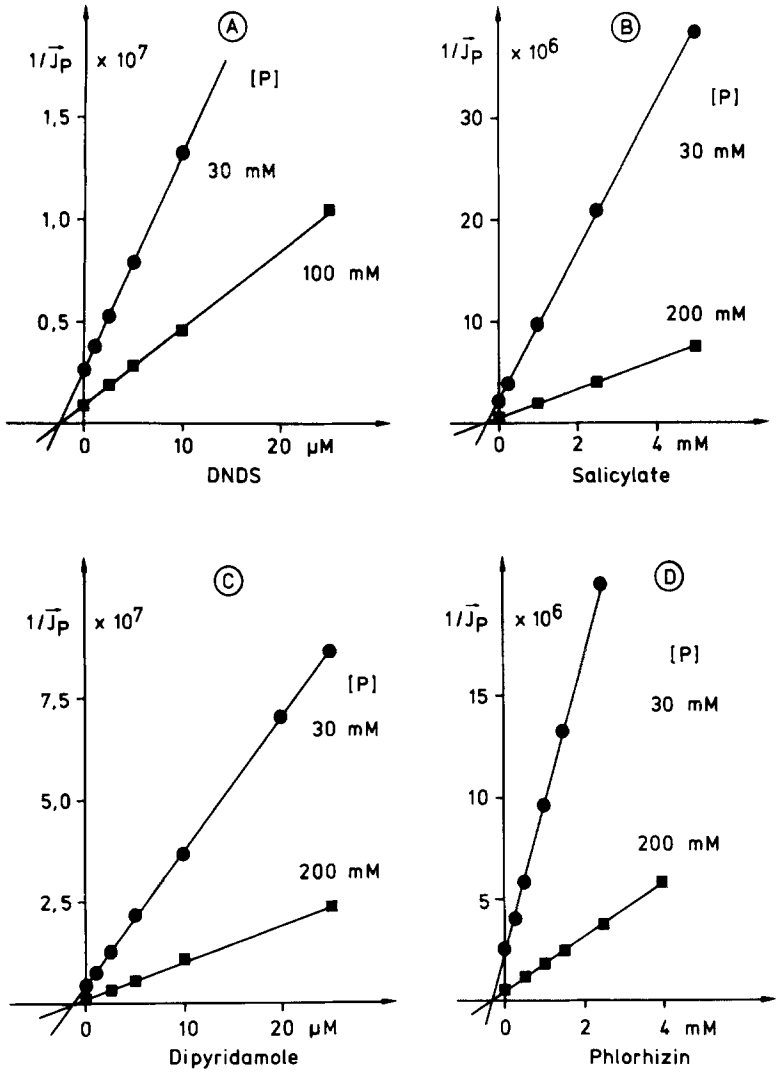

Fig. 9. Dixon plots for DNDS, salicylate, phlorhizin and dipyridamole (20 mM KCl) in resealed erythrocyte ghosts. $\vec{J}_P$ [mol/(min · g cells)] is the unidirectional phosphate flux and [I] the inhibitor concentration. The experiments were carried out with 10% suspensions of resealed erythrocyte ghosts, 25°C, pH 7.2. Phosphate concentrations are indicated in the figure

pattern of inhibition. The apparent inhibition constants, $K_{i(app)}$, and the coordinates of the intersection points for different types of inhibition are given in Table 2. If sufficient data are available, the plot of $\log(i/(i_{max}-i))$ *versus* $\log[I]$ offers some advantages over the Hill-Dixon plot. The plot of $\log(i/(i_{max}-i))$ *versus* $\log[I]$ eliminates self-inhibition and permits a precise determination of i_{max}, the maximal fractional inhibition of the phosphate self-exchange flux. The slope of the double logarithmic plot gives m, the apparent Hill coefficient for inhibitor binding while at $\log(i/(i_{max}-i)) = 0$, the $\log[I]$-axis position provides $\log[I]_{0.5}$ (Table 3).

As indicated by the apparent Hill coefficients, the cooperativity of the phosphate self-exchange flux in amphothericin B permeabilized red cells, is much higher than in resealed erythrocyte ghosts while the apparent phosphate half-saturation constants in permeabilized cells are smaller than in erythrocyte ghosts. In permeabilized red cells, the apparent Hill coefficient is approximately 1.65 while in erythrocyte ghosts, the apparent Hill coefficient amounts to about 1.15. The apparent phosphate half-saturation constant is approximately 75 mM in permeabilized cells and approximately 125 mM in erythrocyte ghosts while the apparent maximal phosphate self-exchange fluxes in permeabilized erythrocytes and in erythrocyte ghosts are similar in magnitude (Table 4). Amphotericin B has no effect upon the phosphate self-exchange flux, but it increases the cation permeability of the red cell membrane and offers a possibility to reduce intracellular phosphate without introducing a second permeable anion species (Deuticke, Kim & Zöllner, 1973; Schnell et al., 1981). There are several reasons which probably can account for the above differences. The greater Hill coefficients and the smaller phosphate half-saturation constants in permeabilized red cells can arise

from self-inhibition of the phosphate flux in permeabilized red cells. Self-inhibition can result in an overestimate of the apparent Hill coefficient and in an underestimate of the phosphate half-saturation constant and of the maximal flux. In erythrocyte ghosts, self-inhibition is missing. Consequently, erythrocyte ghosts should provide the correct Hill coefficients and the correct phosphate half-saturation constants. As shown in Table 4, the intracellular and the extracellular phosphate concentrations in erythrocyte ghosts are equal, but in permeabilized erythrocytes the intracellular and the extracellular phosphate concentrations are different. In permeabilized erythrocytes at phosphate concentrations of smaller than 50 mM, $[P]_e$ is smaller than $[P]_i$ while at phosphate concentrations of greater than 50 mM, $[P]_e$ is greater than $[P]_i$. The overproportional increase of $[P]_e$ in erythrocytes can induce a counterstimulation of the phosphate transport which accelerates ^{32}P-phosphate efflux from the red cells. In erythrocyte ghosts, when the intracellular and the extracellular phosphate concentrations are equal, cooperativity of the phosphate self-exchange is less pronounced. Therefore, the apparent Hill coefficients are smaller and the phosphate half-saturation constants are greater than in permeabilized red cells (Schnell et al., 1981; Schnell & Besl, 1984). The flux measurements of the phosphate self-exchange flux in erythrocyte ghosts have been executed in the presence of 40 mM K-citrate which is required for the resealing of the erythrocyte ghosts. Because of the low substrate specificity of the band 3 substrate site and because of the low affinity of phosphate to the band 3 substrate site, citrate acts as a competitive inhibitor and increases the apparent phosphate half-saturation constant. Phosphate flux measurements in erythrocyte ghosts provided inhibition constants of approximately 200 mM for total citrate (pH 7.2, 25°C). Correcting the apparent phosphate half-saturation for the inhibition by citrate, we end up with phosphate half-saturation constants in the range of 100–120 mM which agree fairly well with those from permeabilized erythrocytes.

In contrast to erythrocyte ghosts, permeabilized red cells show a flux-optimum of the phosphate self-exchange flux at about 150–200 mM phosphate. The addition of chloride or of sulfate shifts the flux-optimum towards higher phosphate concentrations and at 100 mM of chloride or of sulfate the flux-optimum gets lost. In erythrocyte ghosts, phosphate concentrations up to 600 mM have been used, but no self-inhibition of the phosphate flux has been found irrespective of whether isosmotic substitution has been made by sucrose or by K-citrate. To date, the disappearance of the self-inhibition in erythrocyte ghosts is not completely understood. According to the carrier concept of anion transport, self-inhibition of the phosphate flux is attributed to the binding of a second phosphate anion to the band 3 modifier site. It seems unlikely that the modifier site is lost throughout preparation of erythrocyte ghosts, but we cannot exclude with certainity that osmotic hemolysis induces irreversible conformational changes of membrane proteins. As will be discussed below, self-inhibition of the phosphate flux can be caused by the effects of ionic strength upon phosphate translocation. In erythrocyte ghosts, the relative changes of ionic strength are smaller and the apparent phosphate half-saturation constants are greater than in permeabilized erythrocytes and self inhibition therefore may get reduced.

A comparison between phosphate and chloride self-exchange in erythrocytes and erythrocyte ghosts exhibits great differences between chloride and phosphate transport. Chloride self-exchange is approximately 3–4 orders of magnitude faster than phosphate self-exchange. Moreover, chloride and phosphate self-exchange are distinguished by their pH dependency. Phosphate self-exchange exhibits a bell-shaped pH response with a maximum at about pH 6.5 while chloride self-exchange increases from about pH 6 to about pH 7.5 where the flux/pH curves pass through a flat pH optimum. Chloride self-exchange in erythrocytes exhibits saturation kinetics, but at certain conditions, chloride transport also displays a slight sigmoidicity of the flux/concentration curves which seems to be caused by the Donnan distribution of chloride between extracellular and intracellular space. Upon correction for the Donnan effects, the sigmoidicity of the flux/concentration curves is abolished (Gunn et al., 1973; Wieth et al., 1973; Dalmark, 1975, 1976; Brahm, 1977). No differences between chloride self-exchange in intact erythrocytes and in resealed erythrocyte ghosts have been observed (Funder & Wieth, 1976). In contrast to phosphate, the chloride self-exchange in erythrocyte ghosts displays pure saturation kinetics. At 1–100 mM chloride, 40 mM citrate and sorbitol substitution (pH 7.3, 0°C), the flux/concentration curves for the chloride self-exchange in erythrocyte ghosts can be fitted to the Lineweaver-Burke or the Woolf-Augustinsson-Hofstee plot without showing systematic deviations from linearity (Hauntmann & Schnell, 1985).

With regard to phosphate transport, the different plotting procedures indicate controversial patterns of inhibition. The double reciprocal Hill plots for chloride and sulfate show a mixed-type inhibition of the phosphate transport in erythrocyte ghosts and in permeabilized red cells. The Hill-Dixon plots for chloride and for sulfate exhibit a competitive inhibition of the phosphate transport in erythrocyte ghosts

and a mixed-type inhibition of the phosphate transport in permeabilized erythrocytes. In erythrocyte ghosts, the Hill coefficients for chloride and sulfate are close to 1.0 while in permeabilized erythrocytes Hill coefficients of greater than unity for chloride and for sulfate have been obtained. The double reciprocal Hill plots for the concentration dependence of the phosphate self-exchange flux in the presence of the inhibitors, DNDS, salicylate and dipyridamole, display a mixed-type inhibition while the respective Dixon plots exhibit a noncompetitive inhibition of the phosphate self-exchange flux. For phlorhizin, both the double reciprocal Hill plot and the corresponding Dixon plot show the features of a noncompetitive inhibition of the phosphate transport.

Most evidence suggests that the anionic inhibitors, DNDS and salicylate, bind to the band 3 substrate site and elicit a competitive inhibition of the chloride and of the sulfate transport. Detailed studies on inhibition of the chloride transport by DNDS binding have proven that DNDS (4,4′-dinitro-2,2′-stilbene-disulfonic acid, K-salt) is a true competitive inhibitor of the chloride flux (Fröhlich, 1982). This assumption is further supported by our experiments with the stilbene-disulfonic acid spin label, NDS-TEMPO. NDS-TEMPO binding studies show a mutual competition between NDS-TEMPO binding and the binding of chloride, sulfate, DNDS and salicylate. Moreover, NDS-TEMPO elicits competitive inhibition of the chloride and of the sulfate flux (Schnell et al., 1983; Kaufmann, Eberl & Schnell, 1986). Conversely, phlorhizin elicits a mixed-type inhibition of the chloride and of the sulfate transport while dipyridamole induces a mixed-type inhibition of the chloride and a noncompetitive inhibition of the sulfate and of the phosphate transport in resealed erythrocyte ghosts. The inhibition of the phosphate and of the sulfate transport by dipyridamole is mediated by monovalent anions. In the absence of chloride or of other monovalent anions, dipyridamole was found to be completely ineffective (Renner, Dietl & Schnell, 1988; Legrum & Passow, 1989). In contrast to dipyridamole, the inhibitors DNDS, salicylate and phlorhizin are independent of chloride. Phlorhizin and dipyridamole bind to band 3 inhibitor sites which seem to be located in the immediate vicinity of the band 3 substrate site. Independent evidence for the binding of phlorhizin and of dipyridamole close to the band 3 substrate site comes from NDS-TEMPO binding studies. Phlorhizin and dipyridamole both elicit a mixed-type inhibition of the NDS-TEMPO binding and phlorhizin additionally modifies the mobility of membrane bound NDS-TEMPO (K.F. Schnell, *unpublished results*).

Hill coefficients of greater than unity are indicative of a positive cooperativity of the phosphate self-exchange flux. The cooperativity of the phosphate self-exchange flux could result from a cooperativity of phosphate binding, from a cooperativity of phosphate translocation or from both of these effects. A cooperative binding of phosphate requires, at a minimum, two interacting binding sites at the same membrane surface while a cooperative translocation of phosphate requires two interacting binding sites at the opposite membrane surfaces. Previous studies on phosphate transport in erythrocyte ghosts have shown that the positive cooperativity of the phosphate transport can only be observed at self-exchange conditions while at homoexchange conditions the cooperativity of the phosphate transport disappears (Schnell & Besl, 1984). These results suggest a cooperativity of the translocation rather than a cooperative phosphate binding at the membrane surfaces. In addition, the inhibition of the phosphate self-exchange flux by the anion transport inhibitors DNDS, salicylate, phlorhizin and dipyridamole did not provide any evidence for a multi-site transport system. The Hill-Dixon plots for the above inhibitors always provided apparent Hill coefficients of close to unity which is indicative of a single site binding of the inhibitors.

Conversely, the cooperativity of the phosphate self-exchange flux can reflect a participation of electrostatic forces in phosphate binding and in phosphate translocation by a single site. At these conditions, ionizing groups at the band 3 substrate site can be responsible for a cooperative phosphate transport. The study of the concentration dependence of the phosphate self-exchange flux in permeabilized erythrocytes and in erythrocyte ghosts, requires large variations of the concentration of inorganic phosphate which are associated with considerable changes in ionic strength. Ionic strength, s, is given by Eq. (11) where c_i is the concentration and z_i the valency of the ith ion species:

$$s = 0.5\,\Sigma c_i z_i^2. \tag{11}$$

Because of the low substrate-specificity of the band 3 substrate site, no inert spectator anions are available and ionic strength cannot be kept constant. The pK of the second dissociation step of phosphoric acid amounts to 7.21 (25°C) and is equal to the pH at which the experiments have been carried out. Therefore, half the phosphate exists as monovalent $H_2PO_4^-$ and half as divalent HPO_4^{2-}. In permeabilized erythrocytes, phosphate concentrations of 10–400 mM have been employed which corresponds to an ionic strength of 0.02–0.80 M. The addition of 100 mM potassium chloride or of 100 mM potassium sulfate to the phosphate solutions gives an ionic strength of 0.12–0.90 M and of 0.32–1.10 M, respec-

tively. In erythrocyte ghosts, phosphate concentrations of 1–250 mM have been employed and the phosphate solutions were supplemented with 40 mM citrate which is required for resealing. Thus ionic strength in erythrocyte ghosts ranges from 0.226–0.724 M. In the presence of 100 mM potassium chloride or potassium sulfate, ionic strength is in the range of 0.326–0.824 M and of 0.526–1.024 M. These figures indicate that in erythrocyte ghosts, the relative changes of ionic strength are smaller than in permeabilized erythrocytes. For the dose-response curves of chloride and sulfate, changes in ionic strength are smaller, but even then considerable changes of ionic strength must be tolerated. The contribution of the anion transport inhibitors, DNDS, salicylate, phlorhizin and dipyridamole, to ionic strength is small and can be neglected.

Changes in ionic strength can modify the binding of phosphate and of inhibitors to the erythrocyte membrane and can either accelerate or inhibit the translocation of phosphate across the erythrocyte membrane. The flux equations of the unidirectional phosphate flux in presence of a competitive and a noncompetitive anion transport inhibitors are given by Eqs. (12) and (13):

$$\vec{J}_P = \frac{k_{p(app)} E_T [P]}{K_{P(app)} (1 + [I]/K_{i(app)}) + [P]} \tag{12}$$

$$\vec{J}_P = \frac{k_{p(app)} E_T [P]}{(K_{P(app)} + [P])(1 + [I]/K_{i(app)})}. \tag{13}$$

$\vec{J}_P$ is the unidirectional phosphate self-exchange flux, $k_{p(app)}$ and E_T are the apparent rate constant for phosphate translocation and the concentration of the anion transporter, $K_{P(app)}$ and $K_{i(app)}$ are the apparent half-saturation constant of phosphate and the apparent inhibition constant, and [P] and [I] are the phosphate and the inhibitor concentrations, respectively. Taking the effects of ionic strength into account and using as an approximation the limiting Debye-Hückel theory, the relations between the apparent constants (subscript app) and the thermodynamic constants (subscript o) read as follows:

$$k_{p(app)} = k_{po} \cdot 10^{-a \cdot \sqrt{s}} \tag{14}$$

$$K_{P(app)} = K_{Po} \cdot 10^{-b \cdot \sqrt{s}} \tag{15}$$

$$K_{i(app)} = K_{io} \cdot 10^{-c \cdot \sqrt{s}} \tag{16}$$

with: $a = 0.509$; b 1.02 $z_p z_e$; $c = 1.02\ z_{ei} z_i$.

z_p and z_e are the effective charge of phosphate and the effective charge of the empty substrate site while z_{ei} and z_i are the effective charge of the inhibitor site and the inhibitor. Substituting $k_{p(app)}$, $K_{P(app)}$ and $K_{i(app)}$ by k_{po}, K_{po} and K_{io}, and introducing $\vec{J}_{max(Po)} = k_{po} \cdot E_T$, the flux equations for the phosphate self-exchange flux can be rewritten as (for details *see*, Webb, 1963, pp. 815–826):

$$\vec{J}_P = \frac{\vec{J}_{max(Po)} \cdot 10^{-a \cdot \sqrt{s}} [P]}{K_{Po} \cdot 10^{-b \cdot \sqrt{s}} (1 + [I]/(K_{io} \cdot 10^{-c \cdot \sqrt{s}})) + [P]} \tag{17}$$

$$\vec{J}_P = \frac{\vec{J}_{max(Po)} \cdot 10^{-a \cdot \sqrt{s}} [P]}{(K_{Po} \cdot 10^{-b \cdot \sqrt{s}} + [P])(1 + [I]/(K_{io} \cdot 10^{-c \cdot \sqrt{s}}))}. \tag{18}$$

A crude estimate of the factors a, b and c can be made by the following considerations. At pH 7.2, half the phosphate exists as monovalent $H_2PO_4^-$ and half as divalent HPO_4^{2-} and z_p; the effective charge of phosphate was set to 1.5. The bulk of evidence suggests that the band 3 substrate site carries a positive electrical excess charge. Therefore, z_e was set to +1 and b amounts to 1.53. Sulfate transport in red blood cells is associated with an H^+-cotransport (Jennings, 1976; Milanick & Gunn, 1982, 1984). Most probably, the proton is required to neutralize the negative excess charge of the sulfate/substrate site complex and to activate the translocation of sulfate. Phosphate transport across the erythrocyte membrane probably is also accomplished by an H^+-cotransport and requires an activation of the phosphate/substrate site complex by H^+. For these conditions, the factor a is equal to 0.509. Competitive anion transport inhibitors bind to the substrate site of band 3 and inhibit substrate-anion binding. Competitive inhibitors of the anion transport carry negatively charged substituents such as carboxylic or sulfonic groups, but it is difficult to predict whether these substituents are required for the binding or for repulsion of substrate-anions. If the anionic groups are involved in inhibitor binding, $c = 1.02$, but if these groups are only involved in substrate-anion repulsion, $c = 0$. Noncompetitive anion transport inhibitors bind to inhibitor sites which are distinct from the band 3 substrate site. If either the inhibitor or the inhibitor site are uncharged, $c = 0$, but if the inhibitor and the inhibitor site carry electrical charges of opposite sign, $c = 1.02$.

Figures 10 and 11 show computer simulations of the phosphate self-exchange flux. For the computer simulation of the phosphate fluxes Eqs. (17) and (18) have been used. The factors a, b and c are given in the legends to the figures. The computer simulations of the phosphate self-exchange fluxes exhibit many features of the experimental phosphate self-exchange flux in erythrocytes and erythrocyte ghosts. The computer-simulated flux/concentration curves

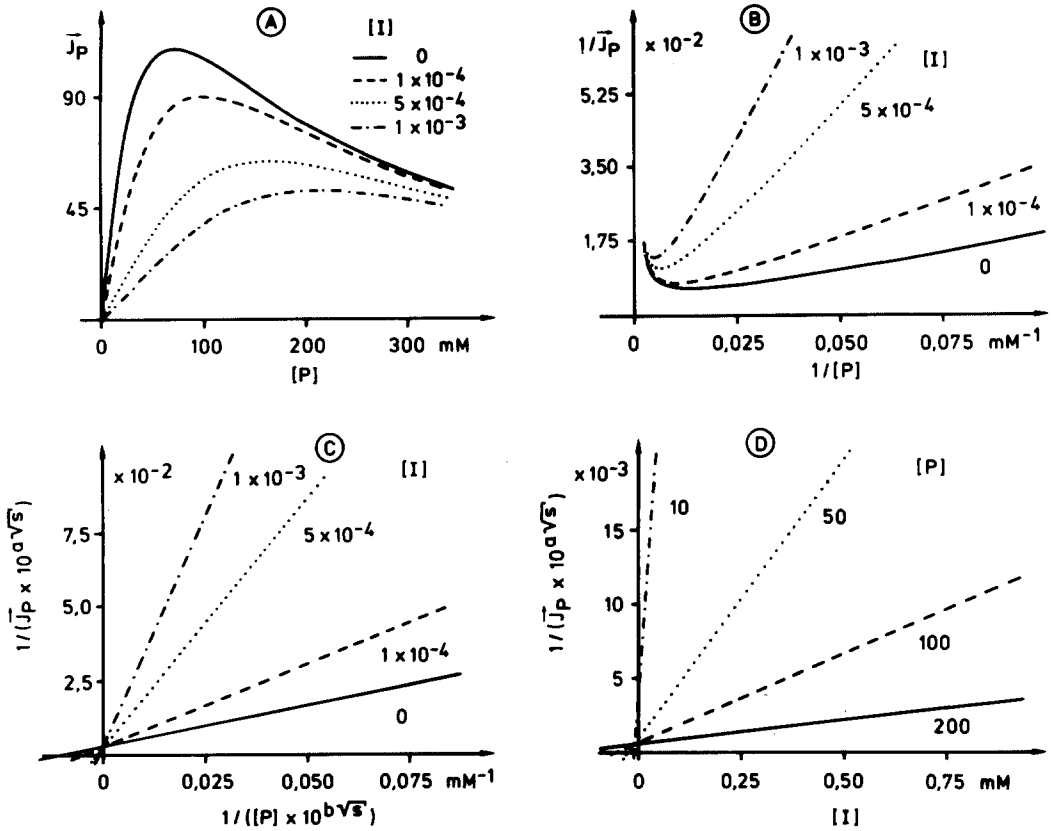

Fig. 10. Computer simulation of the phosphate self-exchange flux in presence of a competitive anion transport inhibitor. (*A*) Flux/concentration curves: $\vec{J}_P$ (a.u.) *versus* [P] (mM). (*B*) Lineweaver-Burk plots: $1/\vec{J}_P$ (a.u.)$^{-1}$ *versus* 1/[P] (mM)$^{-1}$. (*C*) Plots of $1/(\vec{J}_P \cdot 10^{a\cdot\sqrt{s}})$ (a.u.)$^{-1}$ *versus* $1/([P] \cdot 10^{b\cdot\sqrt{s}})$ (mM)$^{-1}$. (*D*) Plots of $1/(\vec{J}_P \cdot 10^{a\cdot\sqrt{s}})$ (a.u.)$^{-1}$ *versus* [*I*] (M). $\vec{J}_P$ (a.u.) is the phosphate self-exchange flux (a.u. = arbitrary units), [P] (mM) and [*I*] (M) are the phosphate and the inhibitor concentration. *s* is ionic strength (M): $s = 0.5\,\Sigma\,(c_i z_i^2)$; c_i (M) is the concentration of the i^{th} ion and z_i is the charge of the i^{th} ion. Phosphate concentrations up to 200 mM and inhibitor concentrations up to 1×10^{-3} M have been used as indicated in the figure. The phosphate self-exchange fluxes have been simulated by means of Eq. (17). Parameters for simulation: $\vec{J}_{max(P)} = 1$ (arbitrary units); $K_{P_o} = 100$ mM; $K_{io} = 1 \times 10^{-4}$ M; $a = 1.0$; $b = 1.53$; $c = 0$. The factors $10^{a\cdot\sqrt{s}}$, $10^{b\cdot\sqrt{s}}$ and $10^{c\cdot\sqrt{s}}$ account for the effects of ionic strength on phosphate translocation, on phosphate and on inhibitor binding, respectively

display an S-shaped concentration dependence, a flux-optimum and a self inhibition at high phosphate concentrations. Competitive anion transport inhibitors shift the flux-optimum towards higher phosphate concentrations, whereas noncompetitive anion transport inhibitors have no effect on the position of the flux-optimum. The Lineweaver-Burk plots for the simulated flux/concentration curves are always curved and self-inhibition is indicated by the increase of $1/\vec{J}_P$ at low 1/[P]. At low phosphate concentrations, the Lineweaver-Burk plots for both competitive and noncompetitive anion transport inhibitors intersect below the origin and cannot be used to distinguish between a competitive and a noncompetitive inhibition.

The effects of ionic strength on the concentration dependence and on the inhibition of the phosphate self-exchange flux can best be demonstrated by the plots of $1/(\vec{J}_P \cdot 10^{a\cdot\sqrt{s}})$ *versus* $1/([P] \cdot 10^{b\cdot\sqrt{s}})$ and by the plots of $1/(\vec{J}_P \cdot 10^{a\cdot\sqrt{s}})$ *versus* $[I] \cdot 10^{c\cdot\sqrt{s}}$ which have been obtained by appropriate transformations of Eqs. (17) and (18). As outlined above, the factors *a*, *b* and *c* account for the effects of ionic strength on phosphate translocation, on phosphate binding and on inhibitor binding, respectively. If phosphate binding and phosphate translocation are independent of ionic strength, the factors *a* and *b* are equal to zero, but if ionic strength is involved in binding and in translocation of phosphate, the factors *a* and *b* are either greater or smaller than zero. For competitive and for noncompetitive anion transport inhibitors, at $c = 0$, the plots of $1/(\vec{J}_P \cdot 10^{a\cdot\sqrt{s}})$ *versus* $1/([P] \cdot 10^{b\cdot\sqrt{s}})$ are linear while at $c = 1.02$, the plots of $1/(\vec{J}_P \cdot 10^{a\cdot\sqrt{s}})$ *versus* $1/([P] \cdot 10^{b\cdot\sqrt{s}})$ are curved. For competitive inhibitors, at $c = 0$, the $1/(\vec{J}_P \cdot 10^{a\cdot\sqrt{s}})$ *versus* $1/([P] \cdot 10^{b\cdot\sqrt{s}})$ plots intersect on the ordinate. At $c = 1.02$, the plots intersect to the left of the ordinate and

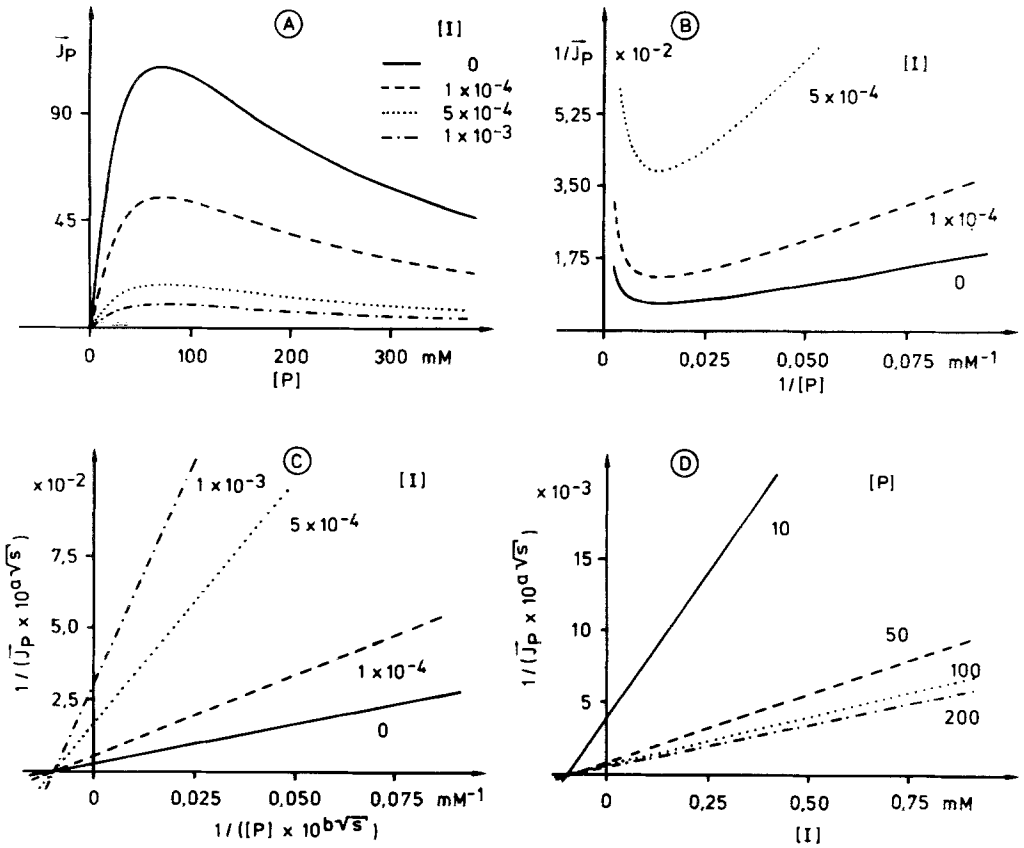

Fig. 11. Computer simulation of the phosphate self-exchange flux in the presence of a noncompetitive anion transport inhibitor. (*A*) Flux/concentration curves: $\vec{J}_P$ (a.u.) *versus* [P] mM. (*B*) Lineweaver-Burk plot: $1/\vec{J}_P$ (a.u.)$^{-1}$ *versus* 1/[P] mM^{-1}. (*C*) Plots of $1/(\vec{J}_P \cdot 10^{a\cdot\sqrt{s}})$ (a.u.)$^{-1}$ *versus* $1/([P] \cdot 10^{b\cdot\sqrt{s}})$ mM^{-1}. (*D*) Plots of $1/(\vec{J}_P \cdot 10^{a\cdot\sqrt{s}})$ (a.u.)$^{-1}$ *versus* [*I*] (M). J_P is the phosphate self-exchange flux in arbitrary units (a.u.), [P] (mM) is phosphate and [*I*] (M) is inhibitor concentration. *s* is ionic strength. The phosphate self-exchange fluxes J_P have been simulated by using Eq. (18). Parameters for computer simulation: $\vec{J}_{max(P)} = 1.0$, $K_{Po} = 100$ mM, $K_{io} = 1 \times 10^{-4}$ M; $a = 1.0$, $b = 1.53$, $c = 1.02$

above the abscissa and have no common intersection point (*not shown*). Conversely, for noncompetitive anion transport inhibitors, at $c = 0$, the plots of $1/(\vec{J}_P \cdot 10^{a\cdot\sqrt{s}})$ *versus* $1/([P] \cdot 10^{b\cdot\sqrt{s}})$ intersect on the abscissa while at $c = 1.02$, the plots give intersection points to the left of the ordinate and below the abscissa (*not shown*). In contrast to flux/concentration curves, dose-response curves are measured at a fixed phosphate and at increasing inhibitor concentrations. Except for substrate-anions the contribution of inhibitors to ionic strength can be disregarded. Therefore the Dixon plots for competitive and for noncompetitive anion transport inhibitors are linear, but the intersection points are shifted by ionic strength towards a lower $1/\vec{J}_P$ and may indicate a wrong pattern of inhibition. The intersection points of the computer-simulated Dixon plots for competitive anion transport inhibitors, are positioned to the left of the $1/\vec{J}_P$-axis and either above or upon the [*I*]-axis (*not shown*) while the intersection points for noncompetitive anion transport inhibitors are located on the [*I*]-axis or below the [*I*]-axis (*not shown*). In order to correct the Dixon plots for ionic strength, the plots of $1/(\vec{J}_P \cdot 10^{a\cdot\sqrt{s}})$ *versus* $[I] \cdot 10^{c\cdot\sqrt{s}}$ can be used where *c* depends on the charge of the inhibitor and of the inhibitor binding site. At $c = 0$, the plots of $1/(\vec{J}_P \cdot 10^{a\cdot\sqrt{s}})$ *versus* [*I*] for competitive inhibitors intersect to the left of the ordinate and above the abscissa while for a noncompetitive inhibitors the intersection point is positioned on the absicssa. At $c = 1.02$, the plots of $1/(\vec{J}_P \cdot 10^{a\cdot\sqrt{s}})$ *versus* $[I] \cdot 10^{c\cdot\sqrt{s}}$ for competitive or for noncompetitive inhibitors intersect to the left of the ordinate and above or below the abscissa.

The effect of ionic strength on the concentration dependence of the phosphate self-exchange flux in erythrocyte ghosts and in permeabilized erythrocytes is shown in Fig. 12. For $a = 0.5$ and $b = 1.5$, the replots of $1/(\vec{J}_P \cdot 10^{a\cdot\sqrt{s}})$ *versus* $1/([P] \cdot 10^{b\cdot\sqrt{s}})$ from the experimental flux/concentration curves provided a much better correlation than for $a = 0$ and $b = 1.5$. These results indicate that both the

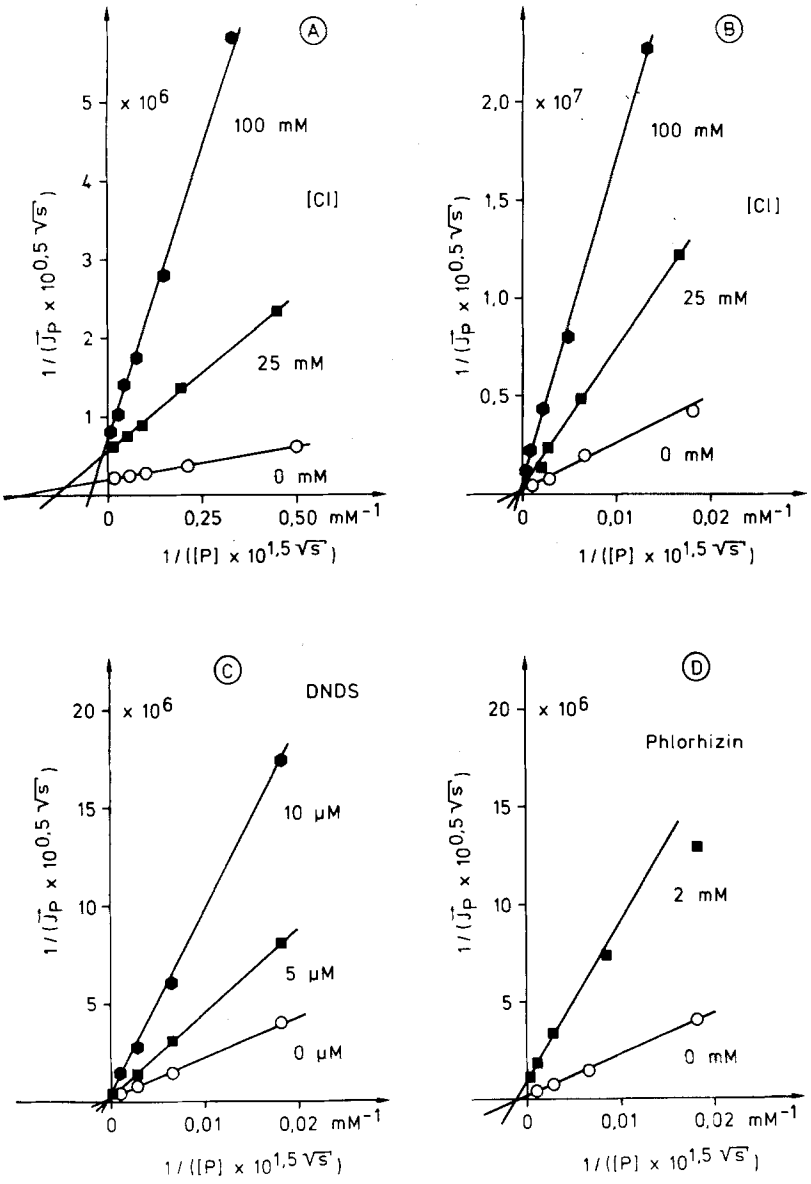

Fig. 12. Replots: $1/(\vec{J}_P \cdot 10^{0.5 \cdot \sqrt{s}})$ *versus* $1/([P] \cdot 10^{1.5 \cdot \sqrt{s}})$. The replots of $1/(J_P \cdot 10^{a \cdot \sqrt{s}})$ $(\text{mol}/(\text{min} \cdot \text{g cells}))^{-1}$ *versus* $1/([P] \cdot 10^{b \cdot \sqrt{s}})$ mM^{-1} have been used to eliminate the effects of ionic strength on phosphate binding and on phosphate translocation. $a = 0.509$ and $b = 1.53$ have been taken from Webb (1963): The factors $10^{a \cdot \sqrt{s}}$, $10^{b \cdot \sqrt{s}}$ and $10^{c \cdot \sqrt{s}}$ account for the effects of ionic strength upon the translocation of phosphate, upon phosphate binding and upon inhibitor binding, respectively. (*A*) Permeabilized erythrocytes: chloride, data from Fig. 3. (*B*) Erythrocyte ghosts: chloride, data from Fig. 2. (*C*) Erythrocyte ghosts: DNDS, data from Fig. 5. (*D*) Erythrocyte ghosts: phlorhizin, data from Fig. 6

translocation and the binding of phosphate are sensitive to ionic strength. In erythrocyte ghosts, the replots of $1/(\vec{J}_P \cdot 10^{0.5 \cdot \sqrt{s}})$ *versus* $1/([P] \cdot 10^{1.5 \cdot \sqrt{s}})$ in the presence of the substrate-anions chloride and sulfate (*not shown*), and in the presence of DNDS and salicylate intersect on the $1/(\vec{J} \cdot 10^{0.5 \cdot \sqrt{s}})$-axis and above the origin. As shown above, these features are indicative of a competitive inhibition of the phosphate self-exchange flux by these inhibitors. In erythrocytes, the replots of $1/(\vec{J}_P \cdot 10^{0.5 \cdot \sqrt{s}})$ *versus* $1/([P] \cdot 10^{1.5 \cdot \sqrt{s}})$ for chloride and for sulfate (*not shown*) are linear and the points from the ascending and from the descending branches of the flux/concentration curves fall on straight lines. The replots of $1/(\vec{J}_P \cdot 10^{0.5 \cdot \sqrt{s}})$ *versus* $1/([P] \cdot 10^{1.5 \cdot \sqrt{s}})$ for chloride and for sulfate in permeabilized erythrocytes intersect to the left of the ordinate and above the abscissa, but the plots have no common point of intersection. Most probably these deviations are caused by contributions of inhibiting anions to ionic strength. The linearity of the replots of $1/(\vec{J}_P \cdot 10^{0.5 \cdot \sqrt{s}})$ *versus* $1/([P] \cdot 10^{1.5 \cdot \sqrt{s}})$ for the flux/concentration curves in permeabilized red cells suggest that ionic strength inhibits the translocation of phosphate and is responsible for the self-inhibition of the phosphate flux. For the inhibitors phlorhizin and dipyridamole (*not shown*), the $1/(\vec{J}_P \cdot 10^{0.5 \cdot \sqrt{s}})$ *versus* $1/([P] \cdot 10^{1.5 \cdot \sqrt{s}})$ replots intersect on the $1/([P] \cdot 10^{1.5 \cdot \sqrt{s}})$-axis and point towards a noncompetitive inhibition of the phosphate self-exchange flux.

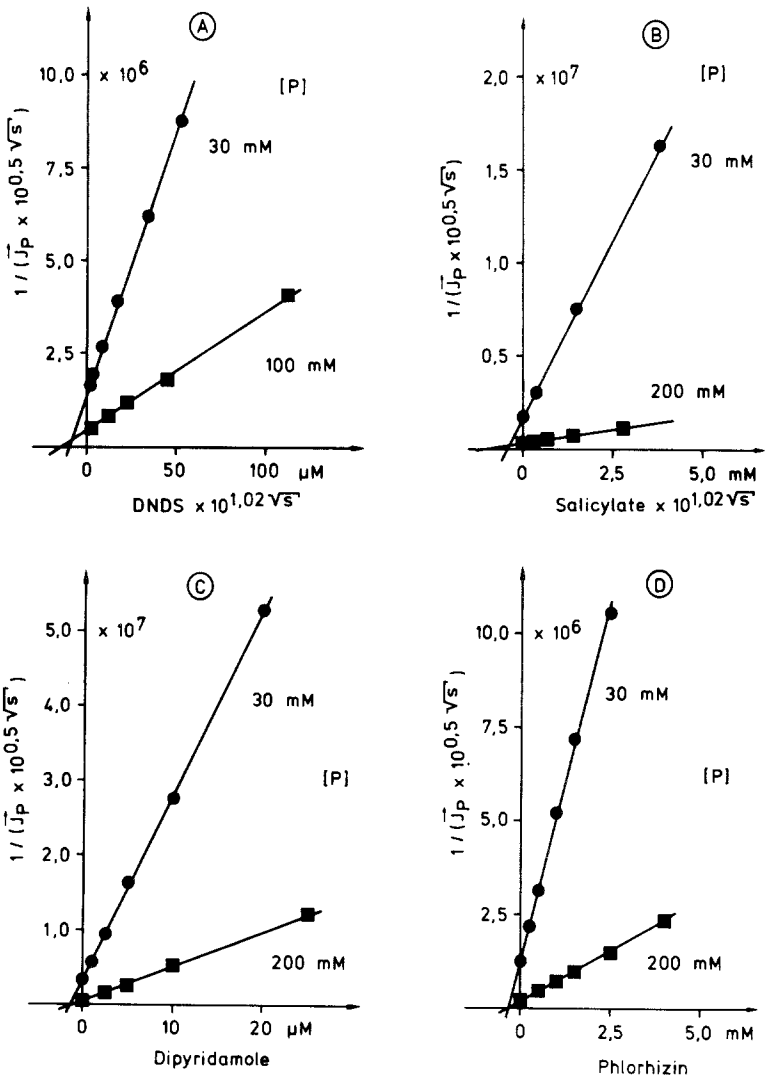

Fig. 13. Replots: $1/(\vec{J}_P \cdot 10^{0.509 \cdot \sqrt{s}})$ *versus* $[I]$ and $1/(\vec{J}_P \cdot 10^{0.509 \cdot \sqrt{s}})$ *versus* $[I] \cdot 10^{1.02 \cdot \sqrt{s}}$ made from the dose-response curves of DNDS, salicylate, phlorhizin and dipyridamole in resealed erythrocyte ghosts. $1/(\vec{J}_P \cdot 10^{0.509 \cdot \sqrt{s}})$ $(\text{mol}/(\text{min} \cdot \text{g cells}))^{-1}$ is the phosphate self-exchange flux corrected for the effects of ionic strength upon phosphate translocation, $[I]$ and $[I] \cdot 10^{1.02 \cdot \sqrt{s}}$ are the inhibitor concentration and the inhibitor concentration corrected for ionic strength effects. The respective Dixon plots are shown in Fig. 9

The effects of ionic strength on inhibitor binding can be tested by the replots of $1/(\vec{J}_P \cdot 10^{a \cdot \sqrt{s}})$ *versus* $[I] \cdot 10^{c \cdot \sqrt{s}}$. At $c = 0$, a linear relation between $1/(\vec{J}_P \cdot 10^{a \cdot \sqrt{s}})$ and the inhibitor concentration $[I]$ should be obtained while for c greater or smaller than zero a linear relation between $1/(\vec{J}_P \cdot 10^{a \cdot \sqrt{s}})$ and $[I] \cdot 10^{c \cdot \sqrt{s}}$ should be obtained. For chloride and for sulfate in permeabilized erythrocytes and in erythrocyte ghosts (*not shown*) and for the anionic inhibitors, DNDS and salicylate in erythrocyte ghosts, the replots of $1/(\vec{J}_P \cdot 10^{0.5 \cdot \sqrt{s}})$ *versus* $[I] \cdot 10^{1.02 \cdot \sqrt{s}}$ are linear and intersect above the $[I] \cdot 10^{1.02 \cdot \sqrt{s}}$-axis (Fig. 13) while the replots of $1/(\vec{J}_P \cdot 10^{a \cdot \sqrt{s}})$ *versus* $[I]$ are curved. Conversely, for phlorhizin and for dipyridamole in erythrocyte ghosts, the replots of $1/(\vec{J}_P \cdot 10^{0.5 \cdot \sqrt{s}})$ *versus* $[I]$ are linear and intersect on the $[I]$-axis (Fig. 13) whereas the replots of $1/(\vec{J}_P \cdot 10^{a \cdot \sqrt{s}})$ *versus* $[I] \cdot 10^{1.02 \cdot \sqrt{s}}$ are curved. These results are suggestive for a competitive inhibition of the phosphate self-exchange flux by DNDS and by salicylate and for a noncompetitive inhibition of the phosphate self-exchange flux by phlorhizin and by dipyridamole.

The participation of electrostatic forces in phosphate binding and in phosphate translocation offers a straightforward interpretation of our experimental results. The effects of electrostatic forces on phosphate binding and on phosphate translocation are indicated by the linear relation between $1/(\vec{J}_P \cdot 10^{a \cdot \sqrt{s}})$ and $1/([P] \cdot 10^{b \cdot \sqrt{s}})$. The band 3 substrate site carries a positive electrical excess charge which facilitates the binding of phosphate and of other anions to the substrate site. The affinity of phosphate to the band 3 substrate site is comparatively low so that electrostatic forces become predominant for phosphate binding. According to the Debye-Hückel the-

ory, increasing salt concentrations reduce the dielectric constant of aqueous solutions and facilitate the binding of phosphate and of H^+ to the band 3 substrate site. These effects seem to be responsible for the sigmoidal concentration dependence of the phosphate self-exchange flux. Conversely, the translocation of bound phosphate across the erythrocyte membrane is activated by the binding of a second proton to the phosphate/substrate site complex of band 3 or to an ionizing group in the immediate vicinity of the band 3 substrate site. The proton seems to be required to counterbalance the negative excess charge of the phosphate/substrate site complex of band 3. At increasing ionic strength, the binding of the second H^+ to the band 3 substrate site is inhibited and as a consequence, the translocation of phosphate across the erythrocyte membrane is reduced. In contrast to substrate-anion binding, the inhibitor binding to the band 3 protein seems to be dominated by short range forces, and, therefore, the effects of ionic strength on inhibitor binding are less pronounced. However, the linear relation between $1/(\vec{J}_P \cdot 10^{a \cdot \sqrt{s}})$ and $1/([P] \cdot 10^{b \cdot \sqrt{s}})$ and between $1/(\vec{J}_P \cdot 10^{a \cdot \sqrt{s}})$ and $[I] \cdot 10^{c \cdot \sqrt{s}}$ provides strong evidence for the assumption that electrostatic forces also participate in the binding of inhibitors. DNDS and salicylate intersect with the band 3 substrate site and elicit a competitive inhibition of phosphate self-exchange flux in erythrocyte ghosts. By contrast, the inhibitor phlorhizin and the chloride-dependent, cationic inhibitor dipyridamole bind to band 3 inhibitor sites in the vicinity of the band 3 substrate site and induce a noncompetitive inhibition of the phosphate transport. For stearic reasons, we cannot exclude a partial overlap of the band 3 substrate site and the band 3 inhibitor sites. Conversely, the inhibitors phlorhizin and dipyridamole can impair the binding of a second H^+ and inhibit the activation of the phosphate/substrate site complex or they can prevent the conformational changes of the band 3 protein which are necessary for the translocation of phosphate. The results of our studies indicate that ionic strength is capable of accounting for many experimental features of the phosphate transport across the erythrocyte membrane.

This work was supported by the Deutsche Forschungsgemeinschaft. We wish to thank M. Dietl and S. Silberhorn for skillful technical assistance. The continuous interest of Prof. Dr. C. Albers and of Prof. Dr. W. Moll in our work is greatfully acknowledged.

References

Brahm, J. 1977. Temperature-dependent changes of chloride transport kinetics in human red cells. *J. Gen. Physiol.* **70**:283–306

Cabantchik, Z.I., Knauf, P., Rothstein, A. 1978. The anion transport system of the red blood cell: The role of membrane proteins evaluated by the use of "probes." *Biochim. Biophys. Acta* **515**:239–302

Cabantchik, Z.I., Rothstein, A. 1972. The nature of membrane sites controlling anion permeability of the human red blood cell as determined by studies with disulfonic stilbene derivatives *J. Membrane Biol.* **10**:311–330

Cabantchik, Z.I., Rothstein, A 1974. Membrane proteins related to anion permeability of human red blood cells: I. Localization of disulfonic stilbene binding sites in proteins involved in permeation. *J. Membrane Biol.* **15**:207–226

Dalmark, M. 1975. Chloride transport in human red cells. *J. Physiol. (London)* **250**:65–84

Deuticke, B., Kim, M., Zöllner, C. 1973. The influence of amphotericin B on the permeability of mammalian erythrocytes to nonelectrolytes, anions and cations. *Biochim. Biophys. Acta* **318**:345–359

Fröhlich, O. 1982. The external anion binding site of the human erythrocyte anion transporter: DNDS binding and competition with chloride. *J. Membrane Biol.* **65**:111–123

Funder, J., Wieth, J.O. 1976. Chloride transport in human erythrocytes and ghosts: A quantitative comparison. *J. Physiol. (London)* **2621**:679–698

Gunn, R.B., Dalmark, M., Tosteson, D., Wieth, J.O. 1973. Characteristics of chloride transport in human red blood cells. *J. Gen. Physiol.* **61**:185–206

Hautmann, M., Schnell, K.F. 1985. Concentration dependence of the chloride selfexchange and homoexchange fluxes in human red cell ghosts. *Pfluegers Arch.* **405**:193–201

Hill, A.V. 1910. A new mathematical treatment of changes of ionic concentration in muscle and nerve under the action of electric currents, with a theory as to their mode of excitation. *J. Physiol. (London)* **40**:190–224

Jennings, M.L. 1976. Proton fluxes associated with erythrocyte membrane anion exchange. *J. Membrane Biol.* **28**:187–205

Jennings, M.L. 1985. Kinetics and mechanism of anion transport in red blood cells. *Annu. Rev. Physiol.* **47**:519–533

Jennings, M.L. 1989. Structure and function of the red blood cell anion transport protein. *Annu. Rev. Biophys. Biochem.* **18**:397–430

Kaufmann, E., Eberl, G., Schnell, K.F. 1986. Characterization of the band 3 substrate site in human red cell ghosts by NDS-TEMPO, a disulfonatostilbene spin probe: The function of protons in NDS-TEMPO and substrate-anion binding in relation to anion transport. *J. Membrane Biol.* **91**:129–146

Knauf, P., 1979. Erythrocyte anion exchange and the band 3 protein: Transport kinetics and molecular structure. *Curr. Top. Membr. Transp.* **12**:251–363

Legrum, B., Passow, H. 1989. Inhibition of inorganic anion transport across the human red blood cell membrane by chloride-dependent association of dipyridamole with a stilbene disulfonate binding site on the band 3 protein. *Biochim. Biophys. Acta* **979**:193–207

Macara, I.G., Cantley, L.C. 1983. The structure and function of band 3. *In:* Methods and Reviews. E. Elson, W. Frazier, and L. Glaser, editors. Vol. 1, pp. 41–87. Plenum, New York

Milanick, M.A., Gunn, R.B. 1982. Proton-sulfate cotransport: Mechanism of H^+ and sulfate addition to the chloride transporter of human red blood cells. *J. Gen. Physiol.* **79**:87–113

Milanick, M.A., Gunn, R.B. 1984. Proton-sulfate cotransport: External proton activation of sulfate influx into human red blood cells. *Am. J. Physiol.* **247**:C247–C259

Passow, H. 1986. Molecular aspects of the band 3 protein-mediated anion transport across the red blood cell membrane. *Rev. Physiol. Biochem. Pharmacol.* **103:**61–203

Renner, M., Dietl, M., Schnell, K.F. 1988. Chloride mediated inhibition of the phosphate and the sulfate transport by dipyridamole in human erythrocyte ghosts. *FEBS Lett.* **238:**77–81

Schnell, K.F. 1977. Anion transport across the red blood cell membrane mediated by a dielectric pore. *J. Membrane Biol.* **37:**99–136

Schnell, K.F., Besl, E. 1984. Concentration dependence of the unidirectional sulfate and phosphate flux in human red cell ghosts under selfexchange and under homoexchange conditions. *Pfluegers Arch.* **402:**197–206

Schnell, K.F., Besl, E., Manz, A. 1978. Asymmetry of the chloride transport system in human erythrocyte ghosts. *Pfluegers Arch.* **375:**87–95

Schnell, K.F., Besl, E., von der Mosel, R. 1981. Phosphate transport in human red blood cells: Concentration dependence and pH-dependence of the unidirectional phosphate flux at equilibrium conditions. *J. Membrane Biol.* **61:**173–192

Schnell, K.F., Käsbauer, J., Elbe, W., Kaufmann, E. 1983. Electron spin resonance studies on the inorganic-anion-transport system of the human red blood cell: Binding of a disulfonatostilbene spin label (NDS-TEMPO) and inhibition of anion transport. *Biophys. Biochim. Acta* **732:**266–297

Tanford, C. 1985. Simple model can explain selfinhibition of red cell anion exchange. *Biophys. J.* **47:**15–20

Webb, J.L. 1963. Enzyme and Metabolic Inhibitors. Vol. 1. Academic Press, New York—London

Wieth, J.O., Dalmark, M., Gunn, R.B., Tosteson, D.C. 1973. The transfer of monovalent inorganic anions through the red cell membrane. *In:* Erythrocytes, Thrombocytes, Leukocytes. E. Gerlach, K. Moser, E. Deutsch, W. Wilmans, editors. pp. 71–76. Stuttgart

Received 18 October 1989; revised 9 April 1990